

Aalborg Universitet



**AALBORG
UNIVERSITY**

Physics Informed Machine Learning for Predicting the Degradation Behavior of Lithium-ion Batteries

Guo, Wendi

DOI (link to publication from Publisher):
[10.54337/aau755548824](https://doi.org/10.54337/aau755548824)

Publication date:
2024

Document Version
Publisher's PDF, also known as Version of record

[Link to publication from Aalborg University](#)

Citation for published version (APA):
Guo, W. (2024). *Physics Informed Machine Learning for Predicting the Degradation Behavior of Lithium-ion Batteries*. Aalborg University Open Publishing. <https://doi.org/10.54337/aau755548824>

General rights

Copyright and moral rights for the publications made accessible in the public portal are retained by the authors and/or other copyright owners and it is a condition of accessing publications that users recognise and abide by the legal requirements associated with these rights.

- Users may download and print one copy of any publication from the public portal for the purpose of private study or research.
- You may not further distribute the material or use it for any profit-making activity or commercial gain
- You may freely distribute the URL identifying the publication in the public portal -

Take down policy

If you believe that this document breaches copyright please contact us at vbn@aub.aau.dk providing details, and we will remove access to the work immediately and investigate your claim.

**PHYSICS INFORMED MACHINE LEARNING
FOR PREDICTING THE DEGRADATION
BEHAVIOR OF LITHIUM-ION BATTERIES**

**BY
WENDI GUO**

PhD Thesis 2024



AALBORG UNIVERSITY
DENMARK

Physics Informed Machine Learning for Predicting the Degradation Behavior of Lithium-ion Batteries

Ph.D. Dissertation
Wendi Guo

PhD Thesis 2024

Submitted: October 2024

Main Supervisor: Associate Professor Daniel Ioan Stroe
Aalborg University

Co-supervisor: Associate Professor Søren Byg Vilsen
Aalborg University

Assessment: Professor Huai Wang (chair)
Aalborg University, Denmark
Professor Daniel Brandell
Uppsala University, Sweden
Professor Andreas Jossen
Technical University of Munich, Germany

PhD Series: Faculty of Engineering and Science, Aalborg University

Department: AAU Energy

ISSN: 2446-1636

ISBN: 978-87-85239-32-7

Published by:
Aalborg University Open Publishing
Kroghstræde 1-3
DK – 9220 Aalborg Øst
aauopen@aau.dk

© Copyright: Wendi Guo

Curriculum Vitae

Wendi Guo



Wendi Guo received her B.Sc. degree in Safety Engineering and M.Eng. degree in Reliability Engineering from Beihang University, Beijing, China, in 2018 and 2021, respectively. She is currently pursuing a Ph.D. at Aalborg University, Denmark, where her research focuses on physics-informed machine learning for prediction of lithium-ion batteries degradation behavior. During her Ph.D. studies, she has held visiting research positions at Chalmers University of Technology in Sweden, and Imperial College London in the UK. She also visited the EES group at Technische Universität München, Germany. Wendi was awarded the Best Poster Award at the 2024 IPEMC ECCE Asia Conference and received a travel grant for early career researchers at the 245th ECS Conference held in San Francisco. She has also actively contributed to the academic community by serving as a reviewer for six top journals and participating in the creation of the white book, "Power Semiconductors for an Energy-Wise Society". Her research interests include packaging reliability of power electronics, lithium-ion battery reliability analysis, digital twins based on multiphysics simulations, and the development of physics-informed machine learning models for battery health prediction.

Curriculum Vitae

Abstract

In recent years, there's been a big push in the transportation and energy sectors towards the use of lithium-ion batteries (LiBs) for their high energy density, efficient charging, long lifetime, and low self-discharge. But as these batteries are used, they degrade, leading to shorter lifetime and potential safety issues. To address this, it's crucial to predict the State of Health (SOH) of LiBs accurately.

However, current methods rely heavily on specific data and lack a deeper understanding of how and why batteries degrade. This PhD project aims to improve the accuracy and applicability of predicting LiBs' degradation, especially for electric vehicle (EV) applications. Instead of relying solely on data like voltage, current, and temperature, a model that combines machine learning with the underlying physics of battery degradation will be developed. This approach enables more reliable predictions of LiB performance over time, improving both efficiency and safety.

Accelerated aging experiments are being conducted on Nickel-Manganese-Cobalt-Oxide (NMC) battery cells to investigate their degradation under varied conditions including fast charging, temperature fluctuations, and dynamic discharging profiles. The aim is to stimulate different dominant mechanisms and generate battery aging dataset. To strike a balance between efficiency and ensuring the consistency of aging mechanisms, careful selection of stress factors is imperative. Extensive calendar and cyclic aging tests have been performed to identify stress rankings and operational intervals for commercial LFP/C batteries using nonlinear mixed effects models. This process aids in the development of testing protocols that enable more accurate prediction of battery lifetime. Subsequently, a test matrix has been devised based on the identified stress factors and aging mechanisms, including SEI layer growth, anode cracking propagation, lithium plating, and electrolyte consumption. These fundamental insights serve as the basis for constructing digital twins and developing physics-informed machine learning algorithms, facilitating a deeper understanding and more precise prediction of battery performance.

Traditional LiB models struggle to accurately predict battery performance under real dynamic conditions, especially considering various aging modes and

mechanisms. To address this limitation, a LiB digital twin is proposed. The digital twin is capable of capturing real measurement data and integrating the intricate coupling between SEI layer growth, anode crack propagation, and lithium plating. The dominant mechanism for the tested NMC532 cells from BOL to EOL is identified as anode particle cracking. This digital twin offers several advantages: it can estimate aging behavior from a macroscopic full-cell level down to a microscopic particle level, including voltage-current profiles in dynamic aging conditions. It enables the prediction of degradation behavior in NMC-based LiBs and supports electrochemical analysis. Moreover, an enhanced digital twin facilitates the quantification of aging effects and identification of aging modes by combining electrochemical techniques with post-mortem analysis to assess chemical and structural degradation. The effectiveness of employing an electrochemical-based digital twin to quantify the impacts of each aging mode and mechanism has been demonstrated, providing a robust physical foundation for physics-informed machine learning in predicting LiB aging behavior.

To address the limitations of black-box models and computationally intensive multiphysics models in predicting LiB degradation, a promising approach is to develop hybrid models that combine physics insights from LiBs' digital twin model with machine learning (ML). A pure machine learning method, called mixed-inputs LSTM, was initially proposed to create a unified model for SOH estimation. To further enhance prediction performance, a strategy called Physics-Informed Neural Network (PINN) was introduced. In this approach, a partial differential equation governing anode particle cracking is used to constrain the neural network (NN) in predicting capacity loss. Compared to baseline NN models, PINN demonstrates improved generalization and accuracy. Specifically, the PINN achieved an average MAE, MAPE, and RMSE of 1.6%, 0.11%, and 1.9%, respectively, compared to 6.1%, 0.42%, and 8.3% for the NN model when using 50% of historical data for retraining.

By exploring digital twin model and physics-informed machine learning rooted in digital twin knowledge, the PhD thesis improves the accuracy and adaptability of battery degradation prediction while minimizing extensive data needs. The outcomes of this Ph.D. project will advance intelligent battery management, charging protocol optimization, and offer valuable insights for the design efforts of next-generation batteries.

Resumé

I de seneste år er der sket en betydelig fremdrift inden for transport- og energisektoren mod anvendelsen af lithium-ion batterier (LiBs) på grund af deres høje energitæthed, effektive opladning, lange levetid og lave selvafladning. Men efterhånden som disse batterier bruges, nedbrydes de, hvilket fører til kortere levetid og potentielle sikkerhedsproblemer. For at imødegå dette er det afgørende at kunne forudsige batteriernes State of Health (SOH) præcist. Nuværende metoder er i høj grad afhængige af specifikke data og mangler en dybere forståelse af, hvordan og hvorfor batterierne nedbrydes. Dette ph.d.-projekt har til formål at forbedre nøjagtigheden og anvendeligheden af LiBs-nedbrydningsforudsigelser, især til elbilapplikationer. I stedet for udelukkende at stole på data som spænding, strøm og temperatur, udvikles en model, der kombinerer maskinlæring med den underliggende fysik af batterinedbrydning. Denne tilgang muliggør mere pålidelige forudsigelser af LiBs' ydeevne over tid og forbedrer både effektiviteten og sikkerheden.

Accelererede aldringseksperimenter udføres på Nickel-Manganese-Cobalt-Oxide (NMC) battericeller for at undersøge deres nedbrydning under varierende forhold, herunder hurtigopladning, temperaturudsving og dynamiske afladningsprofiler. Målet er at stimulere forskellige dominerende mekanismer og generere et dataset for batterialdring. En omhyggelig udvælgelse af stressfaktorer er afgørende for at balancere effektiviteten og sikre sammenhæng i aldringsmekanismerne. Omfattende kalendermæssige og cykliske aldringstests er blevet udført for at identificere stressranger og driftsintervaller for kommercielle LFP/C-batterier ved brug af ikke-lineære mixed effects-modeller. Disse indsigter danner grundlaget for udviklingen af testprotokoller, der gør det muligt at forudsige batteriets levetid mere præcist.

Traditionelle modeller for LiBs har svært ved at forudsige batteriydeevne under dynamiske forhold, især med hensyn til forskellige aldringstilstande og mekanismer. For at imødegå denne begrænsning foreslås en digital tvilling af LiBs. Den digitale tvilling er i stand til at indfange reelle måledata og integrere den komplekse sammenkobling mellem SEI-lagvækst, anodekrakpropagation og lithiumpladning. Den dominerende mekanisme for de testede NMC532-celler fra begyndelse til slutning er identificeret som anodepar-

Resumé

tikelkrakning.

For at håndtere begrænsningerne ved sorte bokse-modeller og komplekse multiphysik-modeller til at forudsige LiBs-nedbrydning er det foreslået at udvikle hybridmodeller, der kombinerer fysikindsigt fra LiBs' digitale tvilling med maskinlæring. Først blev en maskinlæringsmetode kaldet mixed-inputs LSTM foreslået for at skabe en samlet model til vurdering af SOH. Derefter blev en Physics-Informed Neural Network (PINN) strategi introduceret, hvor en partial differential equation om anodekrakpropagation bruges til at begrænse den neurale netværksforudsigelse af kapacitetstab.

Dette ph.d.-projekt vil fremme intelligent batteristyring, optimering af opladningsprotokoller og give værdifulde indsigter til udviklingen af næste generation batterier.

Contents

Curriculum Vitae	iii
Abstract	v
Resumé	vii
Acknowledgements	xi
I Report	1
Chapter 1. Introduction	3
1.1 Background	3
1.1.1 Accelerated Degradation Characterization and Battery Database	4
1.1.2 Physics Based Modelling of Batteries	4
1.1.3 "Grey box" Modelling of Batteries	5
1.1.4 Motivation	7
1.2 Objectives and Limitations	8
1.2.1 Research Question	8
1.2.2 Objectives	9
1.2.3 Limitations	10
1.3 Battery Cell Utilized in This Project	10
1.4 Thesis Outline	11
1.5 List of Publications	12
Chapter 2. Acceleration Degradation Characterization and Battery Database	17
2.1 Identification of aging mechanisms consistency	18
2.1.1 Theory of Mechanism Consistency Discrimination	18
2.1.2 Mechanism Consistency Interval	19
2.1.3 Stress Ranking Comparison	21
2.2 Experimental Setup	24

Contents

2.2.1	Investigated Cell and Material Properties	24
2.2.2	Test Matrix Design	25
2.2.3	Coin cell measurements	25
2.3	Performance Degradation Assessment	26
2.3.1	Electrical Performance	26
2.3.2	Post-mortem Analysis	28
2.4	Summary	31
Chapter 3. Digital Twin-based Degradation Prediction Modelling		33
3.1	Battery Digital Twin Construction	34
3.1.1	Modeling Description	34
3.1.2	Parameter Uncertainty Quantification	38
3.2	Model Validation	40
3.2.1	Capacity and Resistance Prediction	40
3.2.2	Aging Mechanisms Quantification	43
3.2.3	Degradation Diagnosis	46
3.3	Summary	48
Chapter 4. Degradation Prediction Modelling blending ML and Digital Twin Knowledge		49
4.1	Health Status Estimation for Lithium-ion Batteries	50
4.1.1	Data Description	50
4.1.2	Time-series feature extraction	50
4.1.3	Estimation Framework	52
4.1.4	Model performance using multi-input LSTM	52
4.2	Physics-informed Machine Learning for Battery Degradation Prediction	55
4.2.1	Framework overview and flowchart	55
4.2.2	Feature extraction	56
4.2.3	Capacity loss prediction with PINN	59
4.2.4	Impact of Data Ratios on Model Prediction Performance	61
4.2.5	Summary	63
Chapter 5. Conclusions and Future Work		65
5.1	Summary	65
5.2	Main Contributions	67
5.3	Future Research Perspectives	68
	References	70
II Papers		77

Acknowledgements

This PhD research outlines the project’s key findings “Physics-Informed Machine Learning for Predicting The Degradation Behavior of Lithium-ion Batteries.” The project was conducted with the backing of Aalborg University, the China Scholarship Council, and additional support from the Otto Mønsted Foundation.

How time flies! I can hardly believe that I am almost at the end of this challenging yet inspiring PhD journey. I am deeply grateful to my supervisor, mentor, and friend, Assoc. Prof. Daniel Ioan Stroe, who has always supported my unique ideas, my decision to study abroad, carefully reviewed my paper drafts, and encouraged me to run 5 km in the DHL Relay. Although we occasionally had differing opinions and disagreements on research, we were always able to reach a consensus. I also sincerely appreciate his emotional support during a difficult time in my relationship with my ex-fiancé. I am very grateful to my co-supervisor, Assis. Prof. Søren Byg Vilsen, a true mathematical expert and brilliant individual, who supported me in debugging my programming. His invaluable assistance with the development of the PINN and his collaborative spirit greatly advanced my research. He always helped me overcome challenging study issues. Without his guidance, I wouldn’t have been able to complete the machine learning component of my work.

I would like to thank Prof. Torsten Wik and Assoc. Prof. Changfu Zou from Chalmers University of Technology for the insightful discussions and valuable inspiration during my time with the Chalmers ESOC Lab. I am also grateful to Assoc. Prof. Samuel J. Cooper from Imperial College London. His intelligence, energy, kindness, and deep curiosity in both research and humanity have greatly inspired me. He is an excellent mentor and a role model for my future career. I would also like to extend my sincere thanks to my PhD committee for their careful review of my thesis. Your valuable suggestions have greatly contributed to its improvement.

I would like to thank all my friends from my home country and Europe, as well as my colleagues at AAU, for their cherished companionship, inspiration, and shared journey toward growth and success. Special thanks to my sister Yiran Tao, Yaqi Li, Mengfan Zhou, Siyu Jin, Daisy Yu, Ge Lei, Jiaxin Yuan, Yu

Acknowledgements

Fan, Bingxin Yan, and Yuwei Tang for their heartfelt emotional support during my quite difficult and homesick times; their care helped me overcome pain. I also want to express my gratitude to the Be MarS team—an amazing group of ambitious, intelligent, and friendly individuals. We have already achieved great things together, and I look forward to even more success in the future. Thanks to Zhongchao Sun, we have supported each other for eight years, and now it's time to go our separate ways. I wish us both bright futures and hope we each find the right person.

Lastly, I want to thank my parents, who have always supported me, respected every life decision I made, and given me the freedom to pursue my dreams. I will achieve my goals and share my happiness with you both. I would also like to thank myself—a resilient, brave, and determined person who never gives up and always comes back stronger from betrayal and setbacks. You are truly yourself, and you will achieve your goals, find what you desire, and meet a wonderful person.

Now, I am excited and ready to embrace my bright future with confidence and determination.

A handwritten signature in black ink, reading "Wendi Guo". The signature is written in a cursive, flowing style.

Wendi Guo

Aalborg University, October 3, 2024

Part I

Report

Chapter 1

Introduction

1.1 Background

The global surge in demand for lithium-ion batteries (LiBs) is fueled by the rapid adoption of electric mobility and distributed energy storage solutions. Renowned for their high energy density, exceptional charging efficiency, long lifetime, and low maintenance requirements, LiBs have become indispensable in the modern transportation and energy sector [1]. LiBs energy storage technology (EST) is now at the forefront of innovation, driving the future of electric vehicles (EVs). Tesla, for example, uses prismatic cells with LFP chemistry to power its advanced vehicles. Beyond transportation, LiBs play a crucial role in grid stabilization and improving renewable energy integration by serving as effective energy buffers. However, despite their advantages, LiBs gradually lose both capacity and power over time, reducing their lifetime and potentially introducing safety concerns [2]. Addressing these challenges is critical to maximizing their potential in our evolving energy landscape.

The development of LiBs technology faces challenges due to gradual performance degradation (capacity fade, power decrease, etc.), which are critical issues for achieving the long service life required in automotive applications. To tackle these challenges, efforts to extend the lifetime of LiBs have intensified, driving more in-depth studies on battery aging and the development of models to predict degradation. Understanding the physical and chemical processes that cause LiBs to degrade, and combining this knowledge with "big data" analysis to create prediction models, is a complex task. However, overcoming these challenges is essential for advancing LiBs technology.

LiBs are complex systems characterized by non-linear and time-varying properties. Their performance degradation primarily results from electrochemical reactions occurring at the electrodes' level and electrode-electrolyte interface. To better assess the health of LiBs, analyzing these aging mechanisms and developing a digital twin model can be highly beneficial. However, linking

the internal electrochemical parameters to the external input-output responses is challenging due to the intricate internal reactions and varying external environments. This complexity makes physics based modelling difficult. To overcome this, it's crucial to combine physics insights with machine learning (ML). ML can effectively handle non-linear processes and map complex relationships, allowing for the creation of a degradation prediction model that is both adaptive and feasible. This approach ensures the model is guided by physics while also adaptively identifying unknown parameters, ultimately speeding up the prediction process.

1.1.1 Accelerated Degradation Characterization and Battery Database

Degradation prediction modeling for LiBs relies on high-fidelity battery data. Regular testing of LiBs can provide sufficient degradation data; however, this process is both time-consuming and costly. To address this, accelerated degradation tests (ADTs) are an established technique recognized in both industry and academia. ADTs are designed to simulate realistic battery aging over a shorter period by using high-level acceleration factors (AF) such as temperature, C-rate, and depth of discharge (DOD). Data from these tests can then be extrapolated to estimate battery lifetime under normal operating conditions. For ADTs to be effective, it is essential that the dominant degradation mechanisms remain consistent across all stress levels. If not, the extrapolation to normal use conditions may be inaccurate, leading to higher costs in improving battery design and safety. Although ADTs are widely used for battery testing, many tests are guided by expert intuition instead of being grounded in rigorous scientific methodologies [3], [4], [5]. There are limited straightforward and effective methods for verifying the consistency of LiBs' mechanisms, and few guidelines exist for selecting appropriate stress factors and operational ranges. Key challenges include designing ADTs that generate high-quality data for model development and identifying the primary causes of degradation under multiple stress interactions. It is crucial to conduct ADTs with consistent dominant mechanisms and to design a balanced combination of stress factors based on their ranking to ensure reliable results.

1.1.2 Physics Based Modelling of Batteries

Physics-based degradation prediction requires mechanistic analysis and data acquisition to develop an aging model. This method reflects the underlying physical laws, offering the advantage of providing an in-depth understanding of lithium-ion batteries (LiBs) while delivering accurate results. Specifically, there are three primary categories of models: electrochemical models

1.1. Background

(EM) [6], [7], [8], [9], equivalent circuit models (ECM) [10], [11], [12], and semi-empirical models [3], [13], [14].

Electrochemical models offer a detailed understanding of battery behavior, grounded in electrochemical and physical principles to ensure reliability and precision. Among them, the P2D model is the most widely used. However, its complexity introduces challenges, such as high costs and significant computational demands due to complex measurement requirements. To address these limitations, the Single Particle Model (SPM) [15] was developed as a simplified version of the P2D model, focusing on essential battery properties and relying on ordinary differential equations. While this approach improves computational efficiency, it sacrifices the ability to capture nonlinear behavior at high C-rates, as it excludes electrolyte dynamics and the effects of degradation.

Equivalent circuit models are preferred for their conceptual simplicity, which allows easy integration with system-level training algorithms, making them ideal for onboard vehicle applications. These models use lumped parameters and a limited number of variables, enabling users to apply them without a deep understanding of electrochemistry or degradation mechanisms. Instead, users simply need to link the tests from both time and frequency domains to the model's framework. Accuracy, however, can suffer in extreme SOC regions or under high current conditions [16], where the battery's non-linear behavior becomes more evident.

Semi-empirical models establish correlations between stress factors and battery degradation, such as capacity loss or increased impedance, based on data from aging tests conducted under different conditions. Sufficient data is vital for capturing the effects of accelerated calendar and cycle life. These models often rely on time dependence and Arrhenius kinetics [17] in their initial frameworks. To develop semi-empirical models with strong generalization capabilities, it is important to comprehend the model definitions and the physical significance of their parameters. Additionally, selecting appropriate acceleration conditions is crucial for accurate extrapolation.

Table 1.1 presents a detailed comparison of the knowledge requirements, measurement techniques, computational demands, and application characteristics of various physics-based models. This analysis highlights the challenges physical models face in providing accurate and adaptable degradation predictions. As a result, researchers have increasingly turned to hybrid approaches that combine algorithms with different models to overcome these limitations.

1.1.3 "Grey box" Modelling of Batteries

To address the limitations of "black box" models, which lack physical insights, "grey box" models offer a valuable alternative. But why is "grey box" modeling important? "Black box" models heavily depend on the quality of training data. If the data used for training differs from the conditions during testing,

the predictions can be inaccurate or even physically unrealistic. These models require prior exposure to similar conditions to make reliable predictions. In contrast, traditional physical models ("white box") are highly accurate but demand significant computational resources and detailed knowledge of material properties, making them challenging to apply in real-time scenarios. "Grey box" models bridge the gap by combining the strengths of both "black box" and "white box" approaches while minimizing their weaknesses. Two main strategies can be used to integrate data-driven and physics-based methods in a "grey box" model. For more details, refer to [J1].

- Data-driven assisted physical models: Data-driven methods support physics-based models by refining parameters, streamlining first-principle models, and addressing model uncertainties.
- Physics-guided data-driven models: Physical insights are incorporated into the data-driven models by utilizing data with meaningful physical context, accounting for discrepancies between physical models and data-driven predictions, or directly integrating the physical model into the data-driven framework.

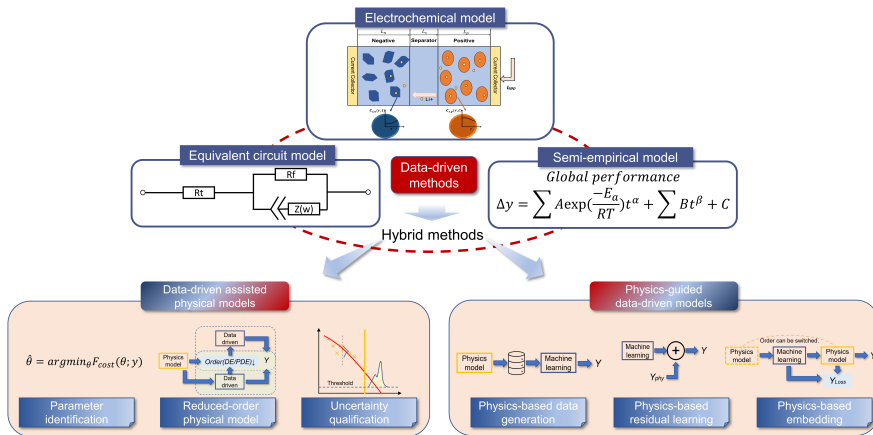


Fig. 1.1: "Grey box" modelling of batteries. Source: [J1].

Combining physical models with data-driven methods has already led to significant improvements in accuracy and practicality. Fig. 1.2(a) illustrates the publication trend up to June 1st, 2022, highlighting the rapid growth of this hybrid method. However, future research should prioritize physics-guided machine learning in prognostics [J1]. With the growing adoption of data-driven algorithms in biology, machine learning is proving to be a highly promising

1.1. Background

tool. In the context of high-dimensional, physically-based models, physics-guided machine learning can estimate parametric functional forms more accurately than traditional techniques such as least squares or other regression techniques. By integrating additional physical crossover factors, this method improves degradation prediction, often requiring the solution of partial differential equations (PDEs) either numerically or approximately. As shown in Fig. 1.2(b), machine learning occupies the largest share of data-driven approaches in "grey box" lifetime modeling. This highlights that machine learning, particularly non-probabilistic methods, is frequently used in conjunction with physics-based models to improve insights into battery aging.

The Physics-Informed Neural Networks (PINN) approach [18] leverages deep learning algorithms to integrate data and solve complex mathematical problems. PINN can compute spatial derivatives in PDEs and handle boundary condition residuals by embedding multi-physics field loss functions into the neural network's loss function. Given the intricate and dynamic nature of lithium-ion battery degradation in electric vehicles, the combination of PINN with electrochemical models or key equations, such as the Butler-Volmer equation and conservation laws, offers a promising pathway for future advancements in battery performance prediction.

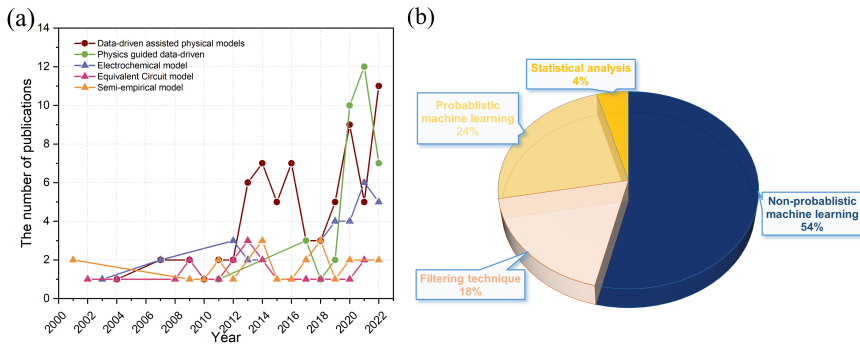


Fig. 1.2: Publication trends reviewed include: (a) distribution across three physical models and two categories of "grey box" battery modeling; (b) percentage breakdown of various data-driven models applied in hybrid methods. Source: [J1].

1.1.4 Motivation

The literature review collates the accelerated degradation tests and forecasting model used for LiB degradation prediction. The focus is on the mechanism consistency interval test condition of ADTs, Multiphysics modelling of battery aging phenomenon, and the improvement of degradation prediction methods.

Considerable studies have been conducted on LiB ADTs, mainly focusing on degradation mechanisms, sensitive parameter capture and test profiles, with insufficient and controversial analysis on the judgement of the rationality of test methodology and the sensitive factors affecting performance deterioration. Based on degradation prediction models, research into the lifetime of LiBs has focused on static or offline conditions, lacking analysis in the case of dynamic operating conditions. There is still potential to study the degradation prediction method of LiBs by combining dynamic loading with different charging/discharging conditions, considering physical properties and internal electrochemical reactions. Sophisticated physical models are not compatible with their practical applications. ML prediction methods cannot describe the internal electrochemical behaviours, limiting their ability to accurately generalize all types of LiBs' lifetime under different operating scenarios. The use of hybrid models combining physical insights and ML to improve the dynamic prediction of online lithium-ion battery degradation is a promising future trend for battery management systems.

This PhD study will contribute to three main areas. Firstly, it should reveal the battery performance deterioration law under different accelerated stress conditions that give suitable accelerated stress levels and their application range. Next, it will bridge the gap between battery degradation prediction models and the study of electrochemical mechanisms, establish and validate the degradation process as a function of external test parameters, and develop a digital twin model with good generalisation capabilities. Finally, an optimised degradation prediction model incorporating ML algorithms with physics insights will be deployed to achieve highly efficient and accurate battery degradation prognostics under dynamic operating conditions.

1.2 Objectives and Limitations

1.2.1 Research Question

The PhD project aims to develop an accurate and adaptive degradation prediction model of LiBs with strong generalization and physics insights. Dynamic lifetime prognosis methods have been studied widely. However, underlying mechanistic outputs and powerful ML tools are not well integrated, leading to cumbersome calculations and poorly transferable online evaluations.

Therefore, the research question of the PhD thesis is:

- **How can ML and physical insights cooperate to produce a physics guided intelligent method to improve the degradation prediction accuracy and adaptability of LiBs?**

1.2.2 Objectives

To answer this question, a set of battery performance data needs to be obtained to provide a credible database. Meanwhile, the main degradation mechanisms should be identified. Furthermore, a physics-informed ML algorithm can be developed. According to the research question, the main objective of this project is:

- **To develop a physics guided ML model that can improve the accuracy and adaptability of dynamic degradation prediction for lithium-ion batteries.**

To achieve this main objective, three technical objectives are considered in the PhD project:

- **Obj1: Accelerated degradation characterization for lithium-ion batteries**

Accelerated degradation conditions and critical stress factors will be determined using reliability accelerated test theory, ensuring a balance between test duration and the consistency of extrapolation mechanisms. Additionally, a test platform will be developed to monitor the characteristics of lithium-ion batteries during degradation. A test matrix will also be designed to stimulate different mechanisms for subsequent model validation.

- **Obj2: Digital twin-based degradation prediction modelling**

The degradation model for lithium-ion batteries will be developed using the integrated P2D model in COMSOL, drawing on previous experimental data and multiphysics simulations to parameterize and identify complex internal parameters. Techniques such as SEM and EDX will be used to characterize underlying physical properties, aiding in model parameterization and validating the mechanisms under consideration.

- **Obj3: Degradation prediction modeling blending machine learning and digital twin knowledge**

A pure machine learning (ML) model will first be used to train a degradation prediction model for benchmarking purposes. Then, ML will incorporate a selected internal electrochemical mechanism to achieve the required accuracy for self-adaptive optimization and dynamic degradation prediction. This physics-informed ML algorithm combines the causal reasoning and deductive strengths of physics-based models with the speed, flexibility, and high-dimensional capabilities of ML.

1.2.3 Limitations

This PhD project still has some limitations, the main ones being:

- The digital twin currently optimizes sensitive parameters using Matlab. However, the optimization process needs to be rerun whenever the parameters are updated. In the future, dynamic optimization should be considered to enable real-time adjustments, allowing the digital twin to actively prolong the service life of the battery cell and battery pack.
- The digital twin model currently does not consider cathode mechanisms because, in the case of NMC532, anode mechanisms are more pronounced. However, to create a more comprehensive model, it is important to include cathode processes such as metal dissolution and particle cracking.
- The physics-informed machine learning method has only been validated on NMC532 cells. To assess its generalization, this method needs to be tested on other NMC configurations as well. Additionally, integrating different mechanisms, beyond just particle cracking, into the machine learning algorithms could enhance their generalizability.

1.3 Battery Cell Utilized in This Project

The cells tested in this study are cylindrical nickel manganese cobalt oxide (NMC) cathode batteries, which are widely used in electric vehicles. The specifications of the tested cells are detailed in Table 1.2. Fig. 1.3 displays the NMC cells being tested in a climate chamber, ensuring consistent ambient temperature control. Voltage, current, and temperature are continuously tracked during the entire testing procedure.

1.4. Thesis Outline

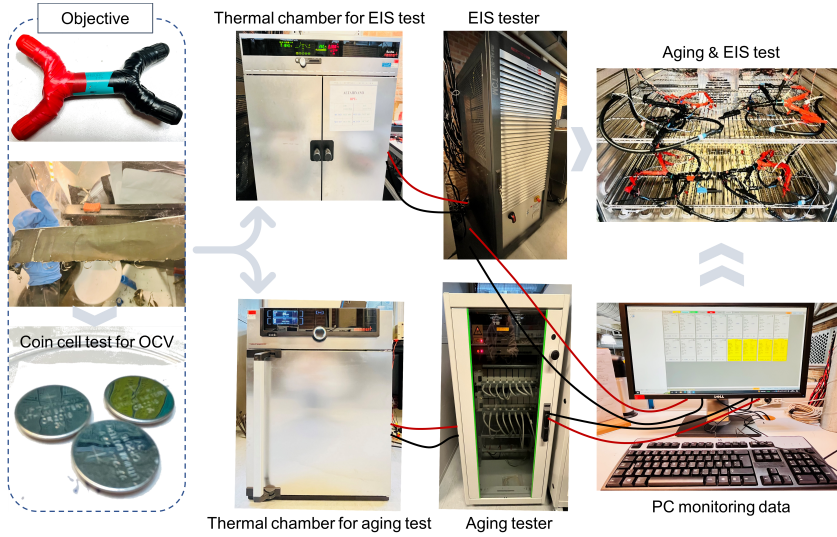


Fig. 1.3: Experiment instruments including operando EIS tester, battery aging tester, temperature chamber and online monitoring PC. Source: supplementary material in [J3].

Table 1.2: Datasheet values of the studied NMC/C battery.

Main Parameter	Value
Model	INR18650-20R
Nominal capacity	2,000 mAh
Nominal voltage	3.6 V
Max. voltage	4.2 V
Min. voltage	2.5 V
Max. continuous discharge current	22 A (at 25°C), 60% at 250 cycles
Operation temperature	-20°C ~ +75°C
Storage temperature	1.5 year: -30°C ~ +25°C

1.4 Thesis Outline

This PhD thesis summarizes the project's outcomes, encompassing a report and selected publications. The thesis structure, shown in Fig. 1.4, consists of five chapters, with relevant papers cited in each. The objectives **Obj 1-Obj 3**

are addressed in Chapters 2-4, respectively.

Chapter 1 opens with an overview of the research background, focusing on accelerated degradation characterization, physics-based modeling, and "grey box" methods. It then highlights the project's motivation, objectives, and limitations. The chapter wraps up by summarizing the thesis structure and presenting the associated publications.

Chapter 2 details the process of selecting suitable accelerated test conditions for experimental design. A test matrix is created based on recommended stress intervals to ensure mechanistic consistency, aiming to activate various degradation mechanisms for model development. The battery cells are tested under varying conditions, including C-rate, temperature, and depth of discharge (DOD). Data on capacity, voltage, current, temperature, and charging time are collected for subsequent modeling and analysis.

Chapter 3 presents the development of a digital twin for lithium-ion batteries, designed to capture real measurement data and model the complex interactions among SEI layer growth, electrolyte consumption, anode crack propagation, and lithium plating. This digital twin can predict aging behavior at both the macroscopic full-cell and microscopic particle levels, including voltage-current profiles under dynamic conditions. It effectively predicts degradation in NMC-based lithium-ion batteries, identifies degradation modes, and supports electrochemical analysis. Furthermore, the model provides critical physical insights, laying the groundwork for physics-informed machine learning algorithm.

Chapter 4 delves into the integration of physical constraints with machine learning models. Initially, a mixed-input LSTM network is explored to assess the health status of battery, accounting for diverse usage patterns, dynamic charging protocols, and limited historical data. Subsequently, the neural network (NN) is enhanced by incorporating partial differential equations that describe anode particle cracking to predict capacity loss. This physics-informed approach outperforms the baseline NN model in terms of generalization, adaptability, and accuracy, especially in scenarios with small sample sizes.

Chapter 5 summarizes the project's conclusions and key contributions. Additionally, it outlines potential directions for future research.

1.5 List of Publications

The dissemination of research from this PhD project is outlined below, including journal papers and conference publications. Several of these, specifically J1-J5 and C1-C4, are incorporated into the PhD thesis.

Journal Papers

- J1. W. Guo, Z. Sun, S.B. Vilsen, J. Meng, D.I. Stroe, Review of "grey box" lifetime modeling for lithium-ion battery: Combining

1.5. List of Publications

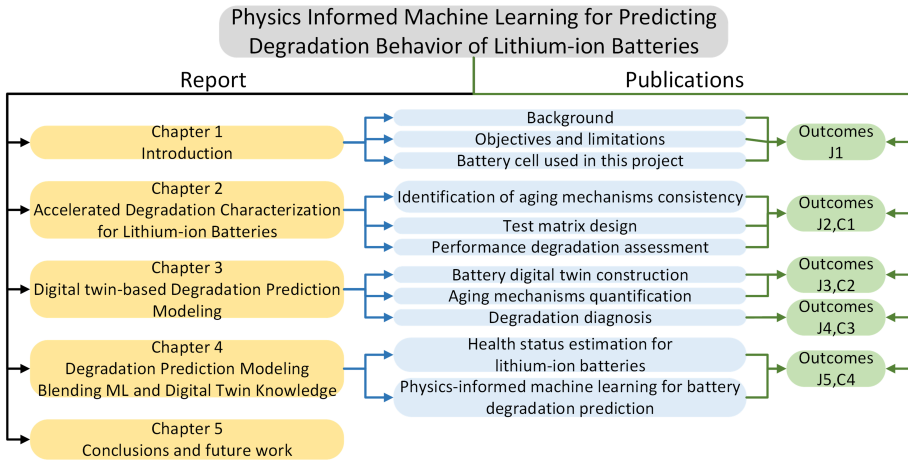


Fig. 1.4: Thesis outline and related publications

physics and data-driven methods, *J. Energy Storage*. 56 (2022) 105992. <https://doi.org/https://doi.org/10.1016/j.est.2022.105992>.

- J2. W. Guo, Z. Sun, S.B. Vilsen, F. Blaabjerg, D.I. Stroe, Identification of mechanism consistency for LFP/C batteries during accelerated aging tests based on statistical distributions, *E-Prime - Adv. Electr. Eng. Electron. Energy*. 4 (2023). <https://doi.org/10.1016/j.prime.2023.100142>.
- J3. W. Guo, Y. Li, Z. Sun, B. Vilsen, D. Ioan, A digital twin to quantitatively understand aging mechanisms coupled effects of NMC battery using dynamic aging profiles, *Energy Storage Mater.* 63 (2023). <https://doi.org/10.1016/j.ensm.2023.102965>.
- J4. W. Guo, Z. Sun, J. Guo, Y. Li, S.B. Vilsen, D.I. Stroe, Digital Twin-Assisted Degradation Diagnosis and Quantification of NMC Battery Aging Effects During Fast Charging, 2401644 (2024) 1–16. <https://doi.org/10.1002/aenm.202401644>.
- J5. W. Guo, Z. Sun, D. I. Stroe, S. B. Vilsen, Physics-informed machine learning for personalized battery capacity loss prediction, in preparation.

Conference Papers

- C1. W. Guo, Z. Sun, Y. Li, S.B. Vilsen, D.I. Stroe, How to identify mechanism consistency for LFP/C batteries during accelerated calendar and cycling aging using the lognormal distribution, *Conf. Proc. - IEEE Appl. Power Electron. Conf. Expo. - APEC. 2023-March (2023)* 1816–1821. <https://doi.org/10.1109/APEC43580.2023.10131387>.

- C2. W. Guo, Y. Li, Z. Sun, S.B. Vilsen, D. Ioan Stroe, Solid electrolyte interface layer growth - crack formation coupled model for Lithium-ion battery capacity fade prediction, 2023 25th Eur. Conf. Power Electron. Appl. EPE 2023 ECCE Eur. (2023).
- C3. W. Guo, Y. Li, Z. Sun, S.B. Vilsen, C. Zou, D.I. Stroe, Diagnosing NMC Battery Aging Modes Using Digital Twin, <https://ecs.confex.com/ecs/245/meetingapp.cgi/Paper/183645>
- C4. W. Guo, Z. Sun, Y. Li, S. Jin, S.B. Vilsen, D.I. Stroe, Health status estimation for lithium-ion batteries with partial charging information using mixed inputs LSTM, 2024 IEEE 10th Int. Power Electron. Motion Control Conf. IPEMC 2024 ECCE Asia. (2024) 1673–1679. <https://doi.org/10.1109/IPEMC-ECCEAsia60879.2024.10567562>.

Other Publications which are not included in the thesis

- J6. Y. Li, W. Guo, D.I. Stroe, H. Zhao, P. Kjær Kristensen, L. Rosgaard Jensen, K. Pedersen, L. Gurevich, Evolution of aging mechanisms and performance degradation of lithium-ion battery from moderate to severe capacity loss scenarios, Chem. Eng. J. 498 (2024) 155588. <https://doi.org/10.1016/j.cej.2024.155588>.
- J7. Z. Sun, W. Guo, A.B. Jørgensen, A Computational Multi-scale Modeling Method for Nanosilver-Sintered Joints with Stochastically Distributed Voids, J. Electron. Mater. 53 (2024) 2437–2454. <https://doi.org/10.1007/s11664-024-10960-x>.
- C5. Y. Li, H. Zhao, W. Guo, F. Blaabjerg, D.I. Stroe, Identification of Lithium-ion Battery Degradation under Fast Charging Protocols, 2024 IEEE Energy Conversion Congress EXPO.
- C6. Z. Sun, M. Takahashi, W. Guo, S. Munk-Nielsen, A.B. Jørgensen, Electro-Thermal Digital Twin for GaN eHEMT Power Modules Temperature Characterization during Power Cycling Tests, 2024 IEEE 10th Int. Power Electron. Motion Control Conf. IPEMC 2024 ECCE Asia. (2024) 4032–4037. <https://doi.org/10.1109/IPEMC-ECCEAsia60879.2024.10567565>.
- C7. S. Jin, X. Yu, X. Sui, W. Guo, M. Bercibar, D.I. Stroe, Features extraction for battery SOH estimation from battery pulsed charging operation, 2023 25th Eur. Conf. Power Electron. Appl. EPE 2023 ECCE Eur. (2023) 1–7. <https://doi.org/10.23919/EPE23ECCEEurope58414.2023.10264335>.

1.5. List of Publications

Table 1.1: Summary of the requirements and key functional features of different physics-based modeling methods. Source: [1].

Models	Requirements	Measurements	Computation	Application
P2D	Knowledge of physical and electrochemical reactions (i.e., PDEs, physical laws)	Geometric parameters (measured using micrometer, SEM, and optical microscopy [19]) Material properties (SEM, XPS, CT [20], and XRD [21]) Diffusion coefficient (GITT and PITT [22]) Resistance value (EIS [23]) Electrochemical analysis (OCV, charge/discharge) Fitted model (dependent on concentration and temperature [24])	An increased number of physical variables and a heavy computational load	Challenging to implement in BMS without simplification Easily transferable to batteries with the same chemistry
SPM	Knowledge of physical and electrochemical reactions (i.e., ODEs, physical laws)	Assumption followed with physical laws [25] Fitted model (dependent on temperature) Similar to P2D measurements	Less computational complexity	Have potential for online use Easily transferable to batteries of the same chemistry Accurate only for low to medium C-rates, as electrolyte physics are not accounted for [26]
ECM	Relationship between model structure and impedance spectrum	Impedance measurements collected through EIS [27] Time-domain analysis (DRT [28]) Electrochemically analysis (charge/discharge, OCV [21]) Fitted Arrhenius behaviors (activation energy obtained from half-cell measurements [29])	Simple structure with effective computation	Easily adapted for on-board circumstances [30] A worse performance, especially in low SOC areas [16] or large current situations
Semi-empirical model	Understanding of power-law relation with time, Arrhenius kinetics, and accelerated tests, preferable some physical insights corresponding to models	Accelerated degradation tests (cycling and calendar aging profiles) Electrical analysis (Capacity, power, or resistance [31])	Heavy sets of experimental research before modeling Speedy computing capability	Simple to implement online Can lead to significant errors [32] unless combined with other physical models [33]

Chapter 2

Acceleration Degradation Characterization and Battery Database

This chapter focuses on establishing a methodology for developing effective test plans to accurately assess lithium-ion battery performance and predict their degradation. A test matrix will be designed according to the recommended operational range and the impact of aging-related stress factors. Experimental tests will then be conducted using this test matrix to simulate different degradation behaviors under various conditions. The resulting datasets will form the basis for developing the subsequent digital twin model and physics-informed machine learning method. The related scientific outcome is outlined as follows:

J2. **W. Guo**, Z. Sun, S.B. Vilsen, F. Blaabjerg, D.I. Stroe, Identification of mechanism consistency for LFP/C batteries during accelerated aging tests based on statistical distributions, *E-Prime - Adv. Electr. Eng. Electron. Energy*. 4 (2023). <https://doi.org/10.1016/j.prime.2023.100142>.

C1. **W. Guo**, Z. Sun, Y. Li, S.B. Vilsen, D.I. Stroe, How to identify mechanism consistency for LFP/C batteries during accelerated calendar and cycling aging using the lognormal distribution, *Conf. Proc. - IEEE Appl. Power Electron. Conf. Expo. - APEC. 2023-March (2023)* 1816 1821. <https://doi.org/10.1109/APEC43580.2023.10131387>.

2.1 Identification of aging mechanisms consistency

2.1.1 Theory of Mechanism Consistency Discrimination

The foundation theory of mechanism consistency discrimination was proposed by Nelson for accelerated testing plans and data analysis [34], [35]. When capacity degradation reaches the failure threshold D_f , the acceleration factor (AF) is defined by the $f(v)$ equation. For more details, refer to [J2]. A higher $AF_{h,l}$ value signifies greater acceleration. The AF depends on the proportion of battery capacity fade (Q_{loss}), except when the power index z remains constant, in which case $AF_{h,l}$ varies with Q_{loss} as follows:

$$AF_{h,l}(Q_{loss}) = \frac{t_l}{t_h} = \frac{\sqrt[z]{f(v_h)}}{\sqrt[z]{f(v_l)}} \times Q_{loss}^{\frac{1}{z_l} - \frac{1}{z_h}}, AF_{h,l} > 1 \quad (2.1)$$

where the subscript l, h indicates lower stress S_l and higher stress S_h [C1], $f(v)$ is the severity coefficient function.

Assume that $F(t; \alpha, \beta, S_l)$ is the lifetime distribution for capacity degradation under stress S_l , following either a Weibull distribution with scale parameter β and shape parameter α , or a lognormal distribution with mean μ_k and variance σ_k^2 [J1]. Then, the parameters need to meet the following conditions to ensure consistency in the aging mechanism:

$$\begin{cases} \alpha^{S_h} = \alpha^{S_l} \\ \beta^{S_l} / \beta^{S_h} = \frac{\sqrt[z]{f(v_h)}}{\sqrt[z]{f(v_l)}} \times Q_{loss}^{\frac{1}{z_l} - \frac{1}{z_h}} \end{cases} \quad (2.2)$$

$$\begin{cases} \sigma_l = \sigma_h \\ \mu_l - \mu_h = \frac{1}{z_h} \ln f_h(v_h) - \frac{1}{z_l} \ln f_l(v_l) + \left(\frac{1}{z_l} - \frac{1}{z_h} \right) \ln Q_{loss} \end{cases} \quad (2.3)$$

As shown in [J1], a parametric bootstrap test likelihood ratio (LR) is used to assess parameter consistency. If lifetime data under varying stress levels are adjusted using Eqs. (2.2) and (2.3), the aging mechanism can be considered consistent if the LR of the distribution remains stable after bootstrapping the adjusted lifetimes across various experimental conditions. The null hypothesis is $H_0 : F(S_l)^C = F(S_h)^C$. The superscript C denotes the corrected lifetime, calculated using either Eq. (2.2) based on the end-of-life (EoL) log-normal assumption, or Eq. (2.3) based on the EoL Weibull assumption, with f representing either the log-normal or Weibull distribution.

$$\Lambda_{obs} = -2 \left(\Lambda_0 - \sum_{i=1}^n \Lambda(f(t_i^c; \eta_i)) \right) \quad (2.4)$$

2.1. Identification of aging mechanisms consistency

$$\Lambda_{boot} = -2 \left[\Lambda_0 - \sum_{q=1}^M \sum_{p=1}^n \Lambda(f(t_{pq}^c; \eta_{pq})) \right] \quad (2.5)$$

where Λ_0 represents a collective model with just two parameters (a common mean and variance, or a common shape and scale) [J2], while Λ_{obs} is the LR calculated between a model accounting for variations in test conditions [C1]. n and m denote the number of accelerated test conditions and random bootstrap tests, respectively. f represents the probability density, and Λ refers to the adjusted lifetime distribution parameters across various accelerated test groups [J2].

2.1.2 Mechanism Consistency Interval

This study was based on commercially available cylindrical 26650 LFP/C battery cells [C1]. Accelerated degradation tests with three key stress factor levels were developed for 43-month calendar aging tests and 10-month cyclic aging tests [36]. These tests provided the battery dataset used to determine the operational range and the impact of aging-related stress factors. Regarding calendar aging, the LR parametric bootstrap test across three temperatures, using both log-normal (Fig. 2.5(a,g)) and Weibull distributions (Fig. 2.5(d,j)) fails the consistency test at a 5% significance level [J2]. (Fig. 2.5). This indicates a change in the calendar aging mechanism within the temperature range of 313.16K to 328.16K. Pairwise tests further reveal that both 313.16K and 328.16K fail, regardless of whether the EoL distribution is log-normal (Fig. 2.5(b,c)) or Weibull (Fig. 2.5(e,f)), pinpointing the mechanism change at 321.66K [J2]. Conversely, LR parametric bootstrap tests across three SOC levels show that the EoL distribution, whether log-normal (Fig. 2.5(g)-(i)) or Weibull (Fig. 2.5(j)-(l)), passes consistently, indicating no significant mechanistic changes [J2]. This suggests that SOC levels ranging from 10% to 90% have minimal influence on the calendar aging mechanism [C1].

As shown in [J2], the LR parametric bootstrap test results for cycling aging across three temperatures, SOC levels, and CD levels are presented in Fig. 2.6 and Fig. 2.7. Under both the EoL log-normal (Fig. 2.7(m-o)) and Weibull distribution (Fig. 2.7(p-r)) assumptions, all three cycle depth (CD) levels and pairwise tests support the consistency of the aging mechanism, showing no significant change in the aging mechanism ranging from 10% to 60% CD [J2]. However, the LR tests fail to support the consistency assumption across various temperatures and SOC levels. For temperatures, LR tests for both log-normal (Fig. 2.6(a)) and Weibull (Fig. 2.6(d)) distributions fail, indicating a mechanism change in the cycling aging range between 308.16 K and 323.16 K. Pairwise tests for temperatures (Fig. 2.6(b,c) for log-normal; Fig. 2.6(e,f) for Weibull) and SOC levels (Fig. 2.7(h,i) for log-normal; Fig. 2.7(k,l) for Weibull) consistently show a

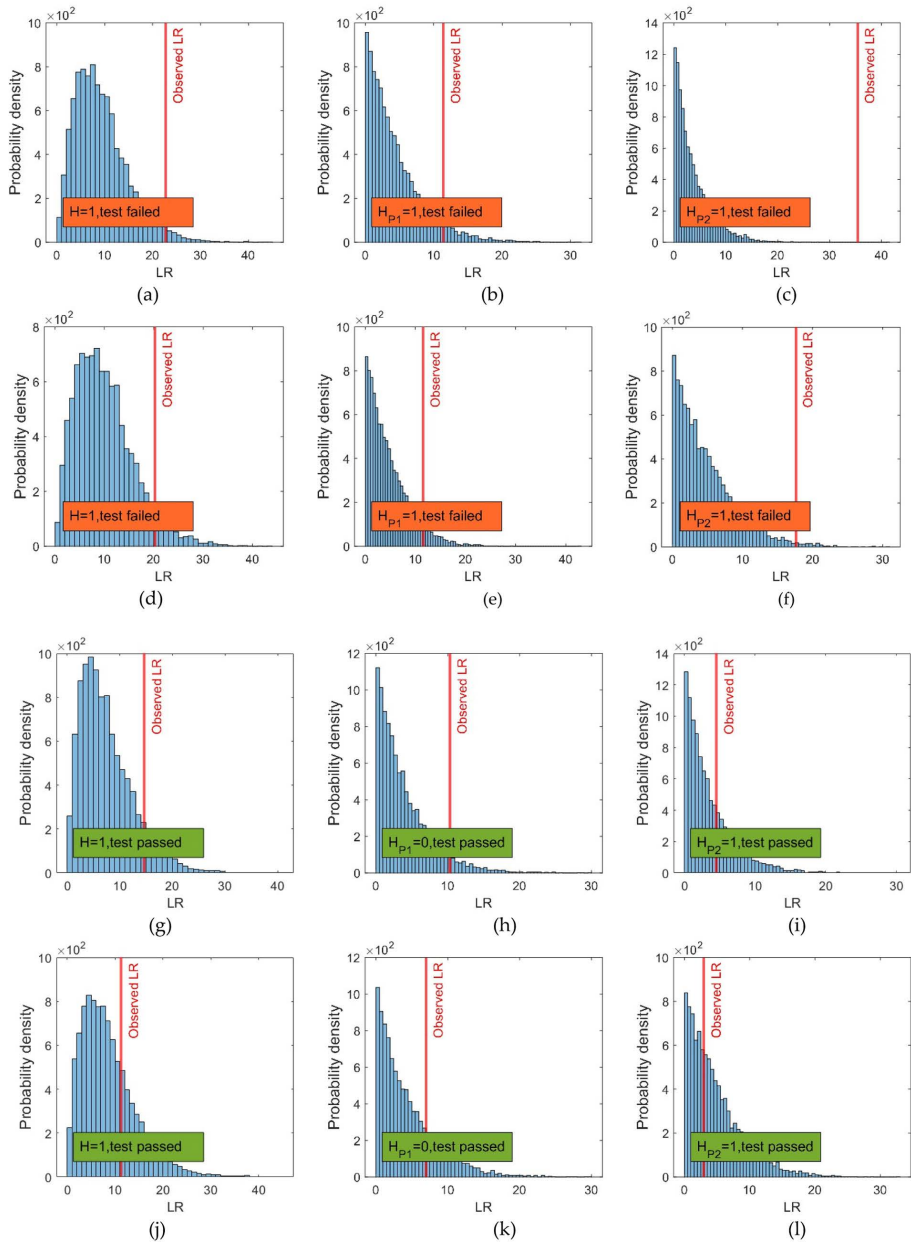


Fig. 2.5: Histogram of LR parametric bootstrap tests at three temperatures using (a-c) log-normal and (d-f) Weibull distributions, and at three SOC levels using (g-i) log-normal and (j-l) Weibull distributions. Source: [J2].

2.1. Identification of aging mechanisms consistency

mechanism change at 323.16 K and 72.5% SOC. This aligns with experimental findings that, above 318.16K, the aging mechanism shifts, and SEI film growth is no longer solely limited by anode diffusion [37].

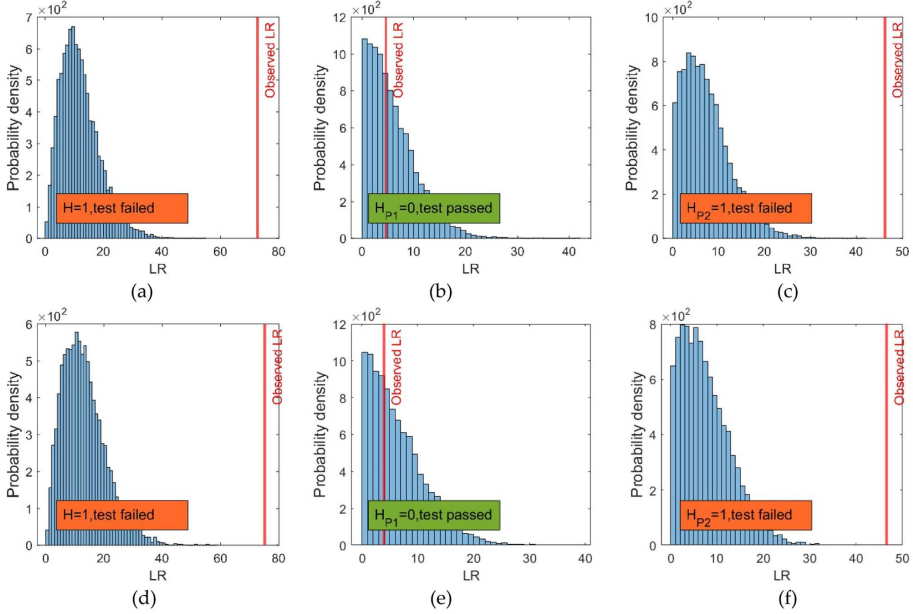


Fig. 2.6: Histogram of LR parametric bootstrap tests at (a-c) three temperatures, (g-i) SOC levels and (m-o) CD levels based on log-normal distribution; (d-f) temperatures, (j-l) SOC levels and (p-r) CD levels based on the Weibull distribution. Source: [J2].

2.1.3 Stress Ranking Comparison

In [C1], parameter interpolation generates a severity factor, $f(v)$, as a function of temperature and SOC, illustrated in Fig. 2.8(a). The SOC level introduces a non-linear factor that amplifies the exponential impact of temperature on calendar aging, though the relationship between SOC and aging is not monotonically increasing. A plateau in capacity degradation is observed around 50% SOC [J2]. It's important to note that the non-linear severity factor is influenced by more than just time. Temperature has the most pronounced impact on aging, as the acceleration factor (AF) at 328.16K and 50% SOC is higher than at 320.66K and 90% SOC [C1]. The acceleration effect is most pronounced at 90% SOC when capacity loss reaches 20%, as shown by the taller bars for 90% SOC under identical temperature conditions.

Fig. 2.9 illustrates the severity factor $f(v)$ alongside the three aging stresses. It also depicts the CD level spanning the effects of temperature and SOC on aging. The sphere volumes in Fig. 2.9(b) represent the AF, with the reference

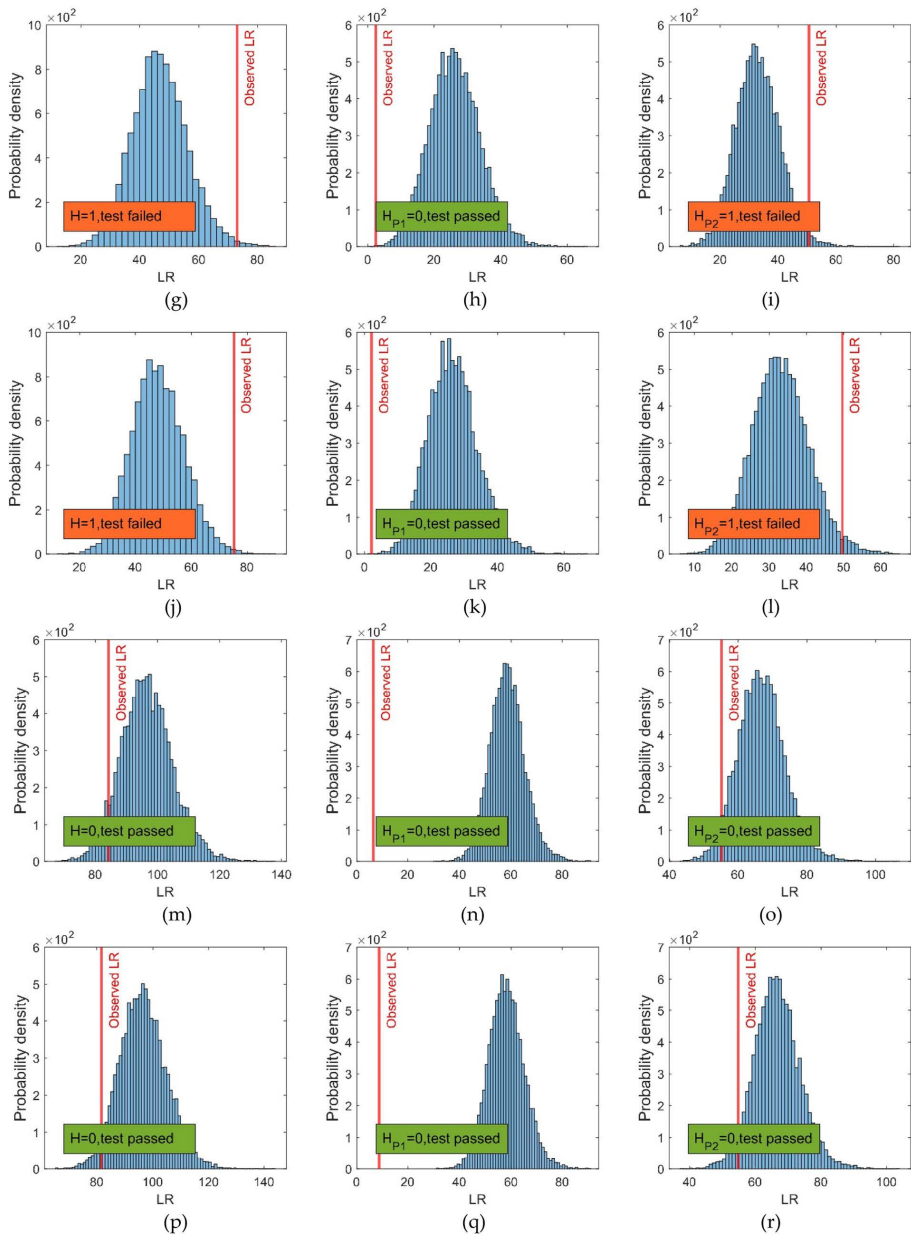


Fig. 2.7: continued

2.1. Identification of aging mechanisms consistency

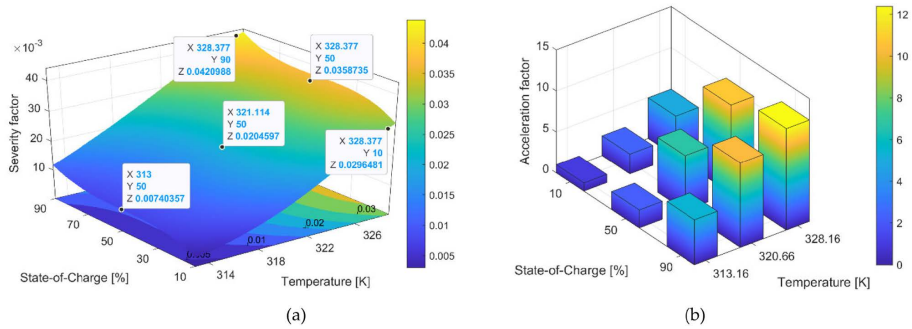


Fig. 2.8: (a) Severity function map for temperature and SOC level. (b) AF for calendar aging stresses at $Q_{loss}=20\%$. Source: [J2].

condition set to $T=308.16\text{K}$, $\text{SOC}=27.5\%$, $\text{CD}=35\%$, and $\text{AF} = 1$. Temperature has the strongest acceleration effect (indicated by red double arrows), followed by the CD level (shown with green double arrows). Notably, the acceleration impact of CD is significantly influenced by temperature, with 323.16K having a much greater effect than 315.66K (highlighted by purple arrows). Lastly, SOC seems to play a minimal role in accelerated cycle aging, though this could be an exception [C1].

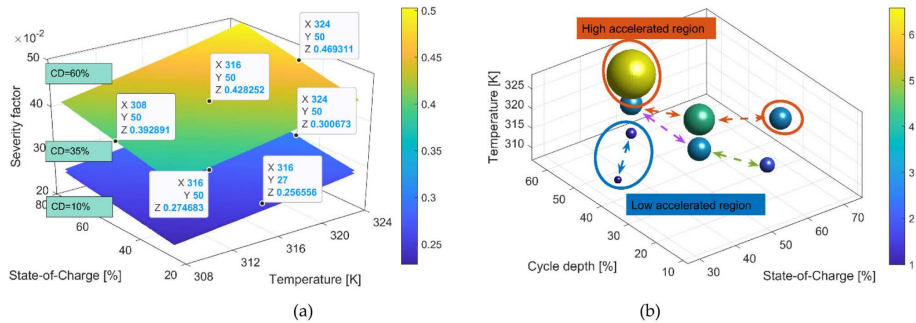


Fig. 2.9: (a) Severity factor map illustrating the impact of temperature and SOC levels. (b) Acceleration factor (AF) for cycling aging stresses at $Q_{loss} = 20\%$. Double arrows represent the comparative analysis used to rank stress levels. Orange, green, and blue colors indicate the effects of temperature, charge/discharge (CD) rates, and combined CD and SOC influences, respectively. Source: [J2].

2.2 Experimental Setup

2.2.1 Investigated Cell and Material Properties

This study utilized commercial INR18650 battery cells. An overview of the material composition and design parameters is provided in Table 2.3. Further details, including the setup for the test sequence, are illustrated in Fig. 2.10.

Table 2.3: Cell design parameters. Source: [J4].

Parameter	Anode	Cathode
Material and Composition	Graphite	NMC 532
Foil Thickness (Ave.) [μm]	82 (meas.)	110 (meas.)
Porosity (Ave.)	0.67 (meas.)	0.69 (meas.)
Electrolyte	LiPF ₆ in a 3:7 by weight EC: EMC	
Separator (Ave.)	18 μm	
Operating voltage (V_{\min} - V_{\max} , V)	2.5-4.2	
Precondition Protocol	5 cycles at C/1 Hold at 3.1 V (\approx 10% SOC)	
Weight (Ave.)	45.0g	

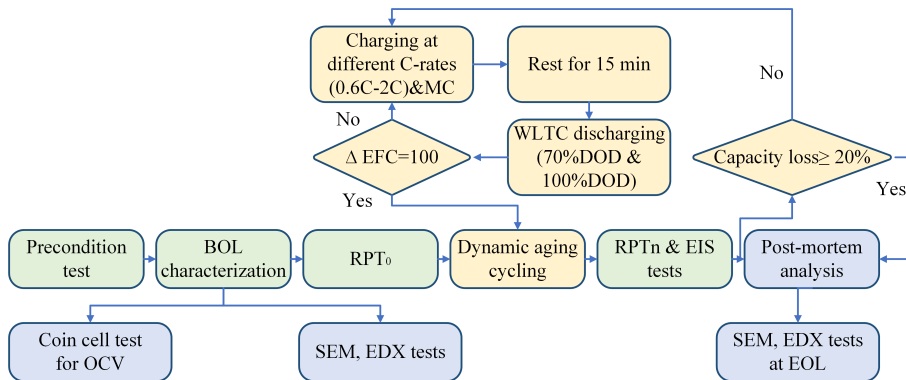


Fig. 2.10: Dynamic aging test sequence. For details on the test platform, refer to [38]. The fast-charging cycles were conducted under 1C to 2C conditions until End of Life (EOL) or under 0.6C until a 10% capacity fade was reached. The tests were carried out over a period of eleven months. Source: supplementary material in [J4].

2.2.2 Test Matrix Design

Sixteen batteries were tested using Neware battery testers (5V12A) across five different aging cycles. During testing, the batteries were charged according to the conditions specified in Table 2.3, while discharging followed the standardized World Harmonized Light Vehicles Test Cycle (WLTC). The WLTC provides a realistic simulation of an EV battery's discharge patterns, reflecting a range of driving conditions, from city traffic to highway speeds, and offering a more accurate depiction of vehicle performance compared to traditional test patterns. Fig. 2.11 illustrates the CCCV charging and WLTC discharging profiles, using 0.6C at 35°C as an example during the degradation process. All tests were conducted in a temperature-controlled environment set to 0°C, 15°C, 25°C, and 35°C. In EV applications, the end-of-life (EOL) for a battery is typically defined as when its capacity drops to 80% of its initial value (BOL). Two batteries were tested for each scenario in this study, except for the 1.3C 25°C and 2C 25°C cases. The remaining two batteries were considered outliers, and their data were not used.

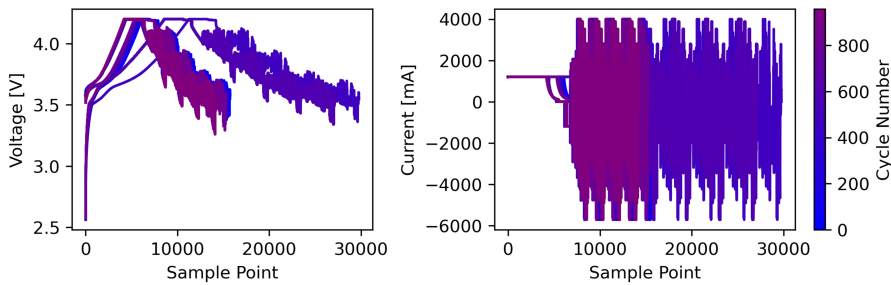


Fig. 2.11: Voltage and current profiles for the 0.6C 35°C case (charging with CCCV, discharging with WLTC).

2.2.3 Coin cell measurements

In [J3], coin cell tests were conducted to obtain the OCV curves and stoichiometry for NMC and graphite electrodes at 0% and 100%. The NMC cathode and graphite anode, taken from freshly disassembled 18650 cells, were paired with a 15 mm lithium metal disc. The electrolyte used was a 1:1 mixture of ethylene carbonate (EC) and diethyl carbonate (DEC) with 1 M LiPF₆. Graphite/Li and NMC/Li coin cells were cycled using a Landt coin cell tester at a constant 0.8 mA current (0.2 C-rate) using a Landt tester. The OCV test data is presented in Fig. 2.12.

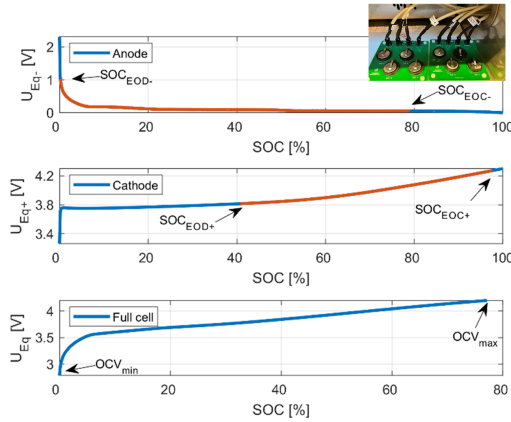


Fig. 2.12: OCV-SOC curves for both fresh electrodes and the full cell, displaying the end-of-discharge (EOD) and end-of-charge (EOC) points, as measured through coin cell experiments. Source: [J3].

Table 2.4: Overview of the test matrix for stimulating anticipated aging mechanisms

NMC532		Temperature (°C)				Major aging mechanisms
		0	15	25	35	
Charging Crate	0.6C	X1, X2			X1, X2	more Li plating
	1C			X1, X2		more SEI growth
	1.3C		X1, X2	X1		
	MC			X1, X2		more cracking
	2C	X1, X2		X1, X2	X1	

2.3 Performance Degradation Assessment

2.3.1 Electrical Performance

A reference performance test (RPT) was conducted at 25°C every 100 EFCs to assess incremental capacity degradation. The cells were charged to 4.2 V using a 0.5 C (1 A) CCCV profile and were considered fully charged once the cut-off

2.3. Performance Degradation Assessment

current dropped to 0.1 A. They were then discharged to 2.5 V at the same constant current. The discharged capacity was used in subsequent analyses to quantify capacity loss over time. Impedance spectra recorded during aging tests (see Fig. 2.13(d,e)) were analyzed using the equivalent circuit model (ECM) in the ZfitGUI software [J3]. Increases in SEI layer resistance and charge transfer resistance are shown in Fig. 2.13(b,c).

Fig. 2.13(a-c) presents the capacity fade of NMC532 cells under seven distinct aging profiles, along with impedance spectrum changes from BOL to EOL. The most significant degradation occurred under the 2C 0°C protocol. For temperatures above 0°C, the 1.3C 15°C protocol exhibited the most pronounced degradation, with a 20% capacity fade within 736 EFCs. Initially, the capacity loss for 2C 25°C and 1.3C 25°C was comparable for the first 500 EFCs, after which the cell aged at 2C experienced accelerated degradation. In contrast, the MC protocol resulted in the least capacity loss, even outperforming the 1C protocol. The lowest capacity loss was observed at 0.6C and 35°C, where an initial capacity increase is attributed to graphite layer expansion, enabling enhanced Li⁺ intercalation, as previously noted in [39]. Fig. 2.13(b,c) compares EIS results at BOL and after 900 EFCs (maintaining a consistent time scale). Initially, the mid and low-frequency semi-circles were similar among cells, with the 2C 25°C cell exhibiting a slightly larger semi-circle. After aging, the 2C 0°C cell showed the fastest increase in charge transfer impedance (R_{ct}). Among the cells aged above 0°C, the highest R_{ct} was observed for the 1.3C 25°C protocol, followed by the 1C, 2C, and MC protocols at 25°C. Fig. 2.13(e) indicates that the increase in R_{ct} for the 2C 35°C 70% DOD protocol was less pronounced, suggesting that lower DOD can reduce the rise in R_{ct} . Fig. 2.13(d,e) also shows changes in R_{SEI} and R_{ct} extracted from ECM parameters, highlighting an accelerated increase in R_{ct} during later aging stages, except under 0°C conditions, which exhibited a decreasing trend. This may be attributed to reduced R_{ct} from lithium metal deposition on the anode surface [40]. R_{SEI} generally increased steadily across all conditions, with a rapid rise under the 2C 0°C protocol and a consistent decline under the 0.6C 0°C protocol. An increase in SEI resistance is associated with dense lithium metal plating [41]. Conversely, the formation of a porous lithium structure and ongoing SEI breakage and reformation could lead to stable or decreasing R_{SEI} values [42].

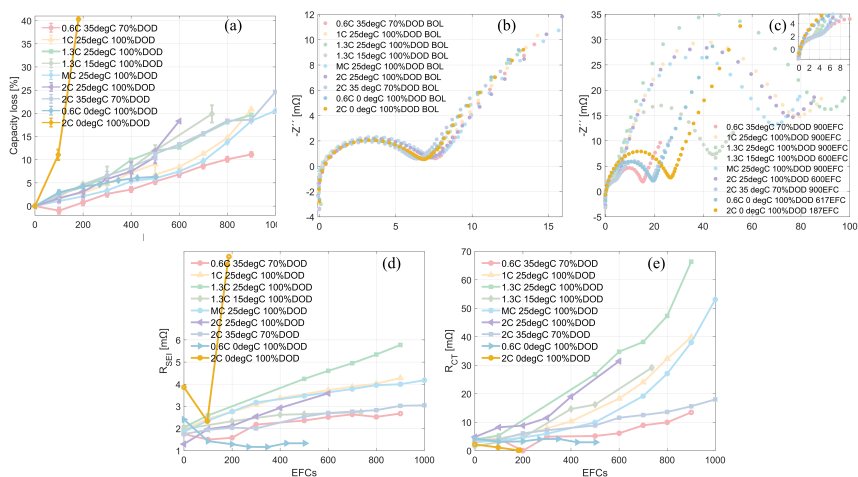


Fig. 2.13: Performance degradation of NMC532 batteries under various fast charging protocols: (a) capacity loss versus EFCs; operando EIS response at (b) BOL and (c) after 900 EFCs; (d) changes in SEI impedance (R_{SEI}); (e) variations in charge transfer impedance (R_{ct}) Source: [J4].

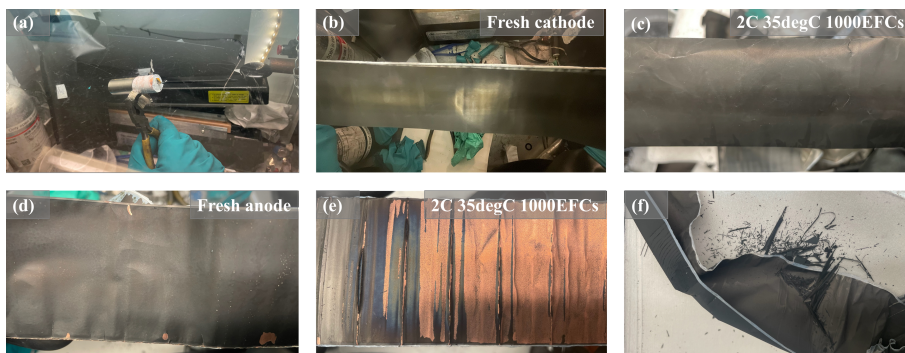


Fig. 2.14: (a) Cell disassembly; (b) Image of fresh cathode; (c) Image of aged cathode; (d) Image of fresh anode; (e) Image of aged anode; (f) Electrode material peeling due to electrolyte consumption. Source: supplementary material in [J4].

2.3.2 Post-mortem Analysis

Aged and fresh cells were analysed to assess loss of lithium inventory (LLI) and loss of active material (LAM). Disassembly revealed non-wet electrodes and peeling of the negative electrode material, suggesting significant electrolyte consumption (Fig. 2.14(f)). As shown in Fig. 2.14(b-e), the fresh electrodes exhibited smooth surfaces, with the positive electrode appearing glossy black and the negative electrode dark gray. In contrast, aged electrodes displayed

2.3. Performance Degradation Assessment

increased surface roughness, particularly on the anode. The yellowish layer on the negative electrode suggests regions rich in SEI layer or lithium, possibly resulting from electrolyte decomposition or lithium plating.

To gain a deeper understanding of the degradation mechanisms, SEM analysis was conducted to examine electrode morphology. The SEM images of cathodes aged under different charging conditions are shown in Fig. 2.15, revealing minimal cathode cracking. In contrast, post-mortem analysis of the anode (Fig. 2.16) confirms the presence of graphite particle cracking. These post-mortem findings are crucial for developing modeling assumptions, identifying relevant degradation mechanisms, and validating the model predictions.

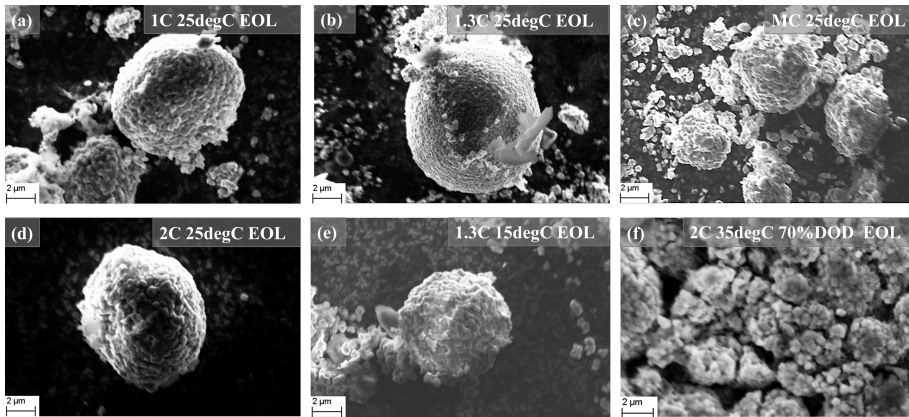


Fig. 2.15: Cathode morphology at end-of-life (EOL) for various conditions: (a) 1C 25°C 100% DOD, (b) 1.3C 25°C 100% DOD, (c) MC 25°C 100% DOD, (d) 2C 25°C 100% DOD, (e) 1.3C 15°C 100% DOD, and (f) 2C 35°C 70% DOD. The 0.6C 35°C 70% DOD cell was not disassembled due to minimal 10% capacity fade. Source: supplementary material in [J4].

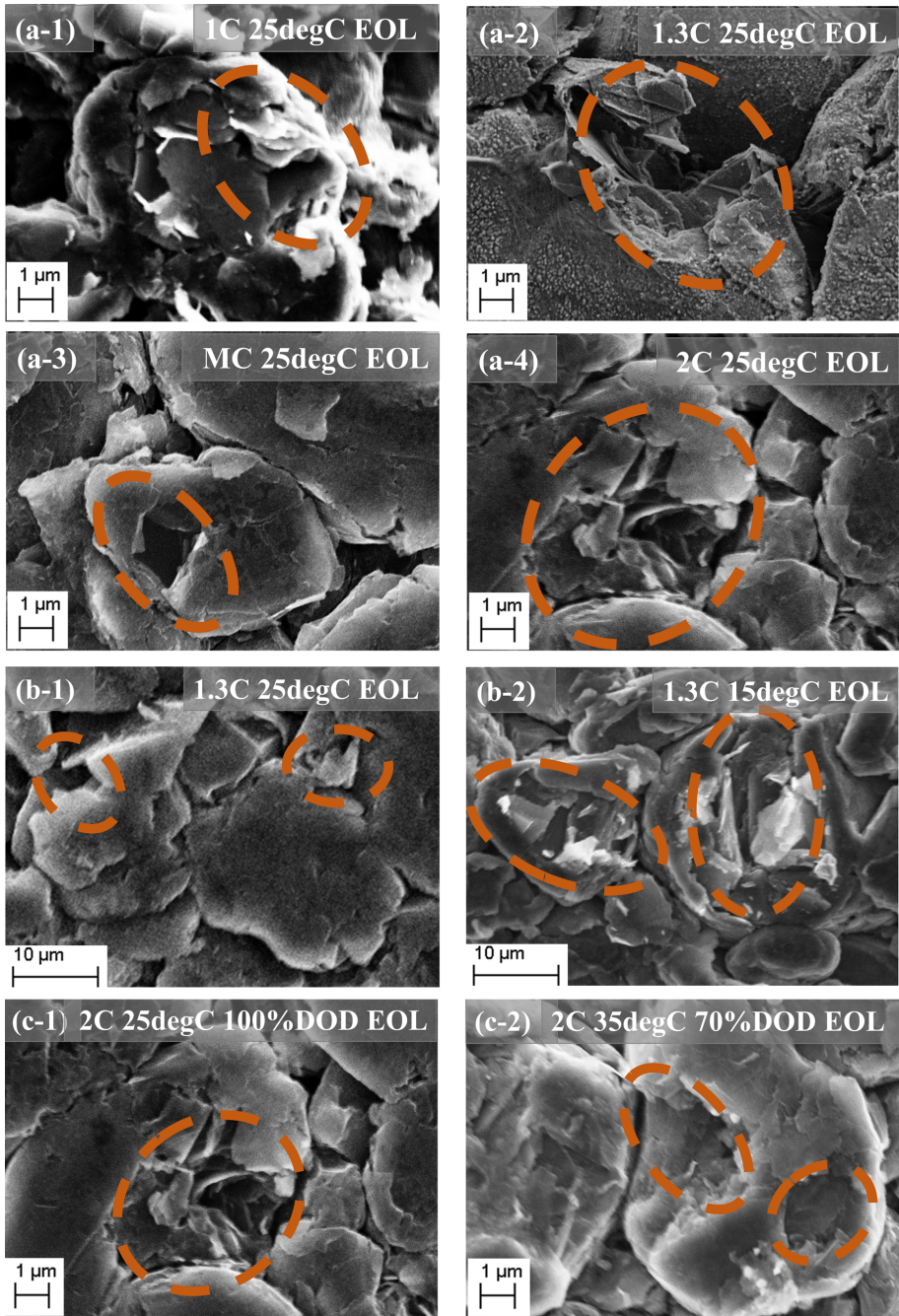


Fig. 2.16: Anode morphology at end-of-life (EOL) for various conditions: (a) 1C 25°C 100% DOD, (b) 1.3C 25°C 100% DOD, (c) MC 25°C 100% DOD, (d) 2C 25°C 100% DOD, (e) 1.3C 15°C 100% DOD, and (f) 2C 35°C 70% DOD. The 0.6C 35°C 70% DOD cell was not disassembled due to a minimal capacity fade of only 10%. Source: supplementary material in [J4].

2.4 Summary

In summary, this chapter explores the suitable test range for aging batteries. Statistical analysis of lithium-ion batteries, based on discharge capacity loss, was conducted to derive the evolution of distribution parameters using a consistent acceleration factor. The likelihood ratio parametric bootstrap method revealed that cycling aging conditions with temperatures above 47.5°C and average SOC levels exceeding 72.5% result in divergent lifetime behaviors. From these insights, seven aging protocols were designed to span from BOL to EOL, ensuring consistent mechanisms for lifetime extrapolation and activating various aging modes for future modeling. The analysis of both macroscopic electrical characteristics and microscopic post-mortem observations identified anode degradation, particularly cracking, as the primary contributor to capacity loss. These findings provide a crucial experimental basis for the development of digital twin model and physics-informed machine learning algorithm.

Chapter 3

Digital Twin-based Degradation Prediction Modelling

This chapter focuses on developing a digital twin for lithium-ion batteries to predict their degradation behavior. The model captures charging and discharging protocols, incorporating the complex interactions of SEI layer growth, anode crack propagation, and lithium plating. The digital twin enables the estimation of aging behavior from the full-cell level down to the microscopic particle scale, providing valuable support for electrochemical analysis of battery degradation mechanisms. This digital twin model establishes a solid basis for developing physics-informed machine learning. The key scientific outcomes are as follows:

J3. **W. Guo**, Y. Li, Z. Sun, B. Vilsen, D. Ioan, A digital twin to quantitatively understand aging mechanisms coupled effects of NMC battery using dynamic aging profiles, *Energy Storage Mater.* 63 (2023). <https://doi.org/10.1016/j.ensm.2023.102965>.

J4. **W. Guo**, Z. Sun, J. Guo, Y. Li, S.B. Vilsen, D.I. Stroe, Digital Twin-Assisted Degradation Diagnosis and Quantification of NMC Battery Aging Effects During Fast Charging, 2401644 (2024) 1–16. <https://doi.org/10.1002/aenm.202401644>.

C2. **W. Guo**, Y. Li, Z. Sun, S.B. Vilsen, D. Ioan Stroe, Solid electrolyte interface layer growth - crack formation coupled model for Lithium-ion battery capacity fade prediction, 2023 25th Eur. Conf. Power Electron. Appl. EPE 2023 ECCE Eur. (2023).

C3. **W. Guo**, Y. Li, Z. Sun, S.B. Vilsen, C. Zou, D.I. Stroe, Diagnosing NMC Battery Aging Modes Using Digital Twin, <https://ecs.confex.com/ecs/245/meetingapp.cgi/Paper/183645>.

3.1 Battery Digital Twin Construction

3.1.1 Modeling Description

A physics model, developed using the pseudo-two-dimensional (P2D) approach, is used to investigate the degradation behavior of NMC-based lithium-ion batteries (LiBs), as published in [J3] and [C2]. Figure 3.17(a) provides an overview of the main electrochemical and parasitic reactions modeled. During discharge, lithium atoms deintercalate from the anode particles, becoming lithium ions that migrate through the electrolyte to the cathode, where they combine with electrons and intercalate as lithium atoms into the layers of the cathode's active material. Parasitic reactions include (1) SEI layer formation, which can occur rapidly before deintercalation starts, within a potential range of 0V to 0.25 V vs. Li⁺/Li. Ethylene carbonate (EC) molecules from the electrolyte diffuse through the outer SEI layer, interacting with lithium ions and electrons in the graphite, resulting in SEI film thickening; (2) lithium plating, which occurs when the overpotential drops below 0V vs. Li/Li⁺; and (3) de/intercalation of lithium ions causes graphite contraction and expansion, leading to anode exfoliation. This process exposes new surfaces, where additional SEI layer formation occurs, as shown in Fig. 3.17(b).

Model Assumption As explained in [J3], the following modeling assumptions are proposed to effectively describe the coupling effects of three considered processes (SEI growth, cracking, and lithium plating).

- Active material particles in both the cathode and anode are modeled as spheres.
- The porous SEI layer is evenly distributed across the graphite/anode surface, maintaining a consistent thickness.
- SEI growth primarily occurs within the stable inner inorganic layer, as the organic layer may shift or undergo further reduction [43].
- Initial cracks on the graphite particles are identical in size and evenly distributed. These cracks propagate inwardly, with their length and density remaining constant.
- Crack propagation is driven by the maximum diffusion-induced cyclic tangential stress resulting from lithium ion intercalation and deintercalation, which continuously impacts the graphite surface.
- The evolution of lithium stripping is not considered in this model.

3.1. Battery Digital Twin Construction

- Thermal effects are accounted for by incorporating temperature-dependent material properties and diffusion coefficients.

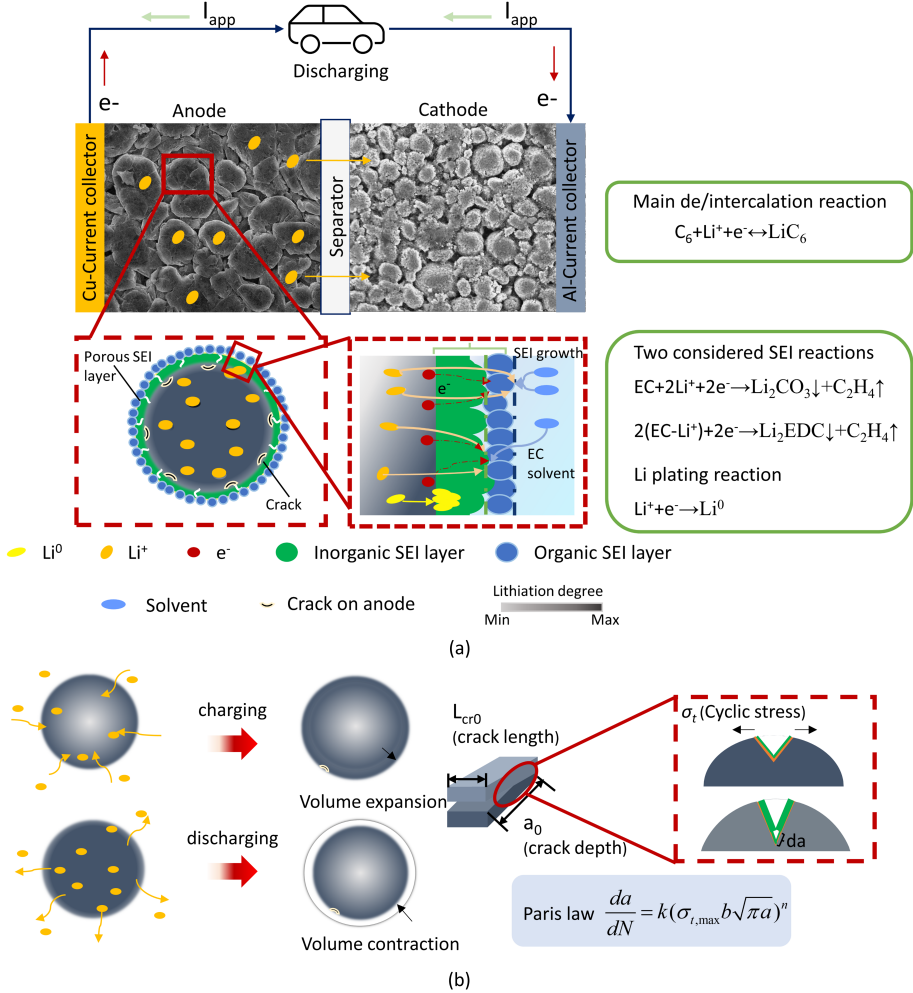


Fig. 3.17: (a) Modeling of primary electrochemical and parasitic reactions; (b) Volume expansion and contraction leading to crack propagation. Source: [J3].

Main intercalation reaction The primary Li^+ intercalation/deintercalation reaction occurs at the particle surface and follows the Butler-Volmer equation [J3], expressed as:

$$j_{int} = j_{int,0} \left[\exp\left(\frac{\alpha_a F}{RT} \eta_{int}\right) - \exp\left(\frac{(1-\alpha_a)F}{RT} \eta_{int}\right) \right] \quad (3.6)$$

where $j_{int,0}$ represents the exchange current density, α_a is the anodic transfer coefficient, and η_{int} indicates the overpotential for the Li⁺ intercalation or deintercalation reaction. The total current density, j_{tot} , is a sum of the intercalation current (j_{int}), SEI formation current (j_{SEI}), and lithium plating current (j_{lpt}): $j_{tot} = j_{int} + j_{SEI} + j_{lpt}$.

SEI layer growth At the first LiB cycle, the SEI layer is formed, and the initial thicknesses of the inner inorganic and outer organic layers are defined as follows [J3]:

$$\begin{aligned} j_0^{inorganic} &= \frac{\delta Q_1 M_{SEI}^{inorganic}}{2A_0 \rho_{SEI}^{inorganic} F} \\ j_0^{organic} &= \frac{(1-\delta) Q_1 M_{SEI}^{organic}}{2A_0 \rho_{SEI}^{organic} F} \end{aligned} \quad (3.7)$$

where A_0 represents the ideal initial surface area of the anode particles. The SEI layer, located at the anode-electrolyte interface, follows the current density of the SEI side reaction as described below:

$$j_{SEI} = - \left[1 + HK_{crd} \left(\frac{C_{n,av}}{C_{n,max}} \right) \right] \frac{J j_{1c,loc} C_{rate}}{\exp \left(\frac{\alpha_a F}{RT} \eta_{SEI} \right) + \frac{Q_{SEI} f}{j_{1c,loc}}} \quad (3.8)$$

where lumped parameters J , H , and f represent the dimensionless exchange current, graphite relative expansion factor, and frequency, respectively [44]. The volume expansion factor, K_{crd} , is associated with the stoichiometric coefficient ($C_{n,av}/C_{n,max}$) in $Li_x C_6$. The SEI reaction overpotential, η_{SEI} , is defined as $\eta_{SEI} = \varphi_s - \varphi_e - U_{eq,SEI}$, where $U_{eq,SEI}$, the SEI reaction equilibrium potential, is set at 0.4 V. The SEI film concentration, C_{SEI} , formed on the anode is determined by mass conservation and is expressed as $\partial C_{SEI} / \partial t = -A_0 j_{SEI} / 2F$. The capacity fade, Q_{SEI} (Ah/ m^2), resulting from SEI layer growth is calculated as follows:

$$Q_{SEI} = \frac{\int_{negative} C_{SEI} \cdot F}{3600} \quad (3.9)$$

Lithium Plating Lithium ion loss from lithium plating is assumed to be irreversible [J3]. Therefore, the current density of the lithium deposition reaction is described using the Tafel equation rather than the Butler-Volmer equation, as follows:

$$j_{lpt} = \begin{cases} -j_{lpl,0} \exp \left(-\frac{\alpha_a j_{pl} F}{RT} \eta_{lpl} \right), & \eta_{lpl} \leq 0 \\ 0, & \eta_{lpl} > 0 \end{cases} \quad (3.10)$$

The current density of lithium plating at the anode particle interface, denoted as $j_{lpl,0}$, is defined by the equation $j_{lpl,0} = k_{lpl} C_l^{\alpha_{lpl}}$, where $\eta_{lpl} = \varphi_s - \varphi_e - j_{tot} R_{film}$ represents the overpotential required to initiate the lithium plating reaction. The deposited lithium concentration, C_{lpt} , is calculated using

3.1. Battery Digital Twin Construction

mass conservation as $\partial C_{lpt}/\partial t = -A_v j_{lpt}/F$. Assuming that lithium plating is irreversible, the capacity loss Q_{lpt} (Ah/ m^2) due to this process is expressed as follows:

$$Q_{lpt} = \frac{\int_{negative} C_{lpt} \cdot F}{3600} \quad (3.11)$$

Crack Formation of Anode Initial cracks on the anode surface grow during cycling due to diffusion-induced stress from lithium ions. As these cracks propagate, they expose more surface area to the electrolyte, leading to continuous SEI formation. Paris' law describes the growth of crack depth as a function of the cycle numbers N [26].

$$\frac{da}{dN} = k(\sigma_{t,max} b \sqrt{\pi a})^n \quad (3.12)$$

The parameters k , b , and n are material-specific constants, with a representing the crack depth and $\sigma_{t,max}$ denoting the peak diffusion-induced tangential stress on the anode particle surface [C2].

Crack propagation impacts the anode's diffusion coefficient; as cracks deepen, the effective diffusion constant of the anode's active material decreases.

$$D_n^{eff}(N) = D_{n,0} \left(1 - \frac{a(N)}{a_{max}}\right)^\beta \quad (3.13)$$

where β is a fitting parameter, and a_{max} represents the maximum allowable anode crack damage, as described in [45].

$$a_{max} = -0.5902 \times \frac{0.7173 + 0.0027 \times r_n - 0.15/r_n}{1 + |0.0223 \times C_{rate} - 10.2115 - 0.002 \times r_n|} \quad (3.14)$$

As there is no crack growth in the first cycle, with only initial SEI formation, the equations for Q_{crack} and Q_{reform} can be integrated to find the solution [J3].

$$Q_{crack}(N) = \frac{2-n}{2} \frac{\Psi}{Z} \left[(1+ZN)^{\frac{2}{2-n}} - (1+Z)^{\frac{2}{2-n}} \right] \quad (3.15)$$

$$Q_{reform}(N) = \frac{K_{SEI,0} \exp\left(-\frac{E_{a,SEI}}{RT}\right) \Psi^{N-1}}{l_0^{inorganic}} \sum_{j=1}^{N-1} (1+Zj)^{\frac{n}{2-n}} (N-j)^{\frac{1}{2}} \quad (3.16)$$

where

$$\psi = \frac{16\pi r_n^2 \rho_{cr} l_{cr,0} k(\sigma_{t,max} b \sqrt{\pi a_0})^n \rho_{SEI}^{inorganic} F l_0^{inorganic}}{\delta_e M_{SEI}^{inorganic}} \quad (3.17)$$

and

$$Z = \frac{2-n}{2} k(\sigma_{t,max} b \sqrt{\pi})^n a_0^{\frac{2}{2-n}} \quad (3.18)$$

3.1.2 Parameter Uncertainty Quantification

The cell voltage significantly impacts seven capacity-related parameters [46]: $C_{s,max}$, L_p , L_n , ϵ_n , ϵ_p , r_n , and r_p . Fig. 3.18(a) shows a Morris One-At-a-Time (MOAT) sensitivity analysis of these parameters, highlighting their impacts on cell voltage. The analysis indicates that the negative electrode porosity (ϵ_{neg}) and positive electrode particle size (r_{pos}) have minimal impact on voltage. Additionally, a global sensitivity analysis of capacity was performed using Sobol indices for the top five MOAT-sensitive parameters. Assuming a normal distribution with a mean of u_i and variance of $0.01 * u_i$, the first-order Sobol indices (left bar) indicate the effect of individual parameters on capacity, while the total Sobol indices (right bar) capture the influence of parameter interactions. Results indicate that $C_{s,max}$ has the greatest influence on capacity, followed by ϵ_{pos} , r_{neg} , and L_{pos} , with L_{neg} having the least effect. Fig. 3.18(c) presents an uncertainty quantification of capacity for these four parameters. Optimization of these four sensitive parameters for voltage and capacity was conducted using dynamic aging protocols, leveraging the integrated P2D model in COM-SOL 6.2. To validate the model, charge voltage curves at every 100 EFCs under various aging conditions were compared with experimental data, as shown in Fig. 3.19. The model demonstrates good agreement with experimental results, with RMSE and MAE below 4% most of the time. The earlier onset of the 4.2V charging voltage indicates irreversible capacity loss with aging. Detailed results (refer to [J4]) confirm that the RMSE and MAE for voltage predictions remain under 4%.

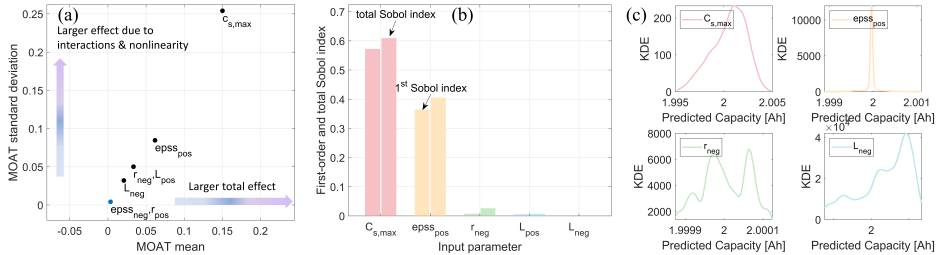


Fig. 3.18: Parameter sensitivity analysis and uncertainty quantification. (a) MOAT method to identify the sensitivity of seven parameters on voltage; (b) Sobol indices for the top five MOAT-effect parameters on capacity; (c) Uncertainty quantification on capacity of top four Sobol indices effect parameters. Source: [J4].

3.1. Battery Digital Twin Construction

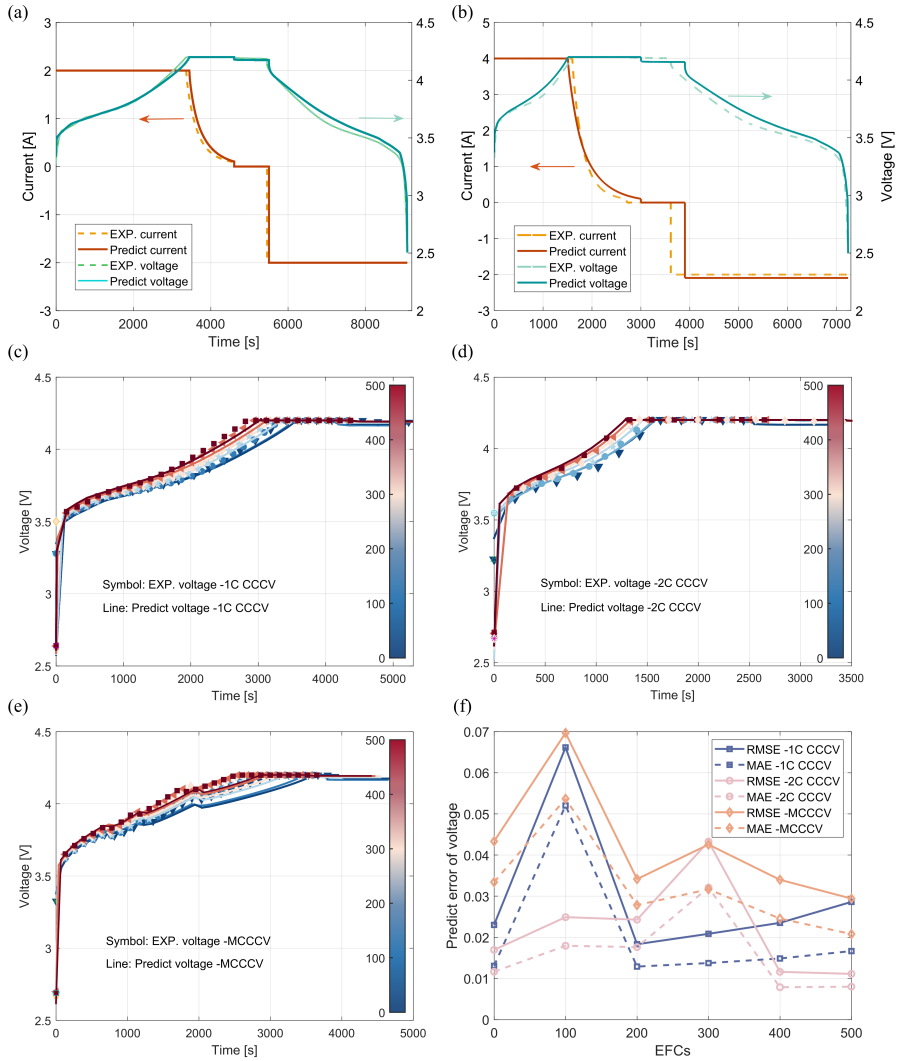


Fig. 3.19: Optimized current and voltage responses used to calibrate the physics model for CCCV protocol: (a) 1C and (b) 2C charging protocols. (c-e) Comparison of model results with test data, showing charging voltage vs. EFCs during cycling aging. (f) Voltage error across the three charging protocols. Source: [J3].

3.2 Model Validation

3.2.1 Capacity and Resistance Prediction

The overall framework proposed for predicting the battery degradation is illustrated in Fig. 3.20. Using aging tests and measured battery parameters, a proposed digital twin accurately predicts battery aging behavior, addressing the three considered aging mechanisms. Insights from this model are then used to propose an optimized charging profile to extend the NMC battery's service life [J3]. The critical step involves building a digital twin for the LiBs and adjusting SEI growth and crack parameters for accurate predictions.

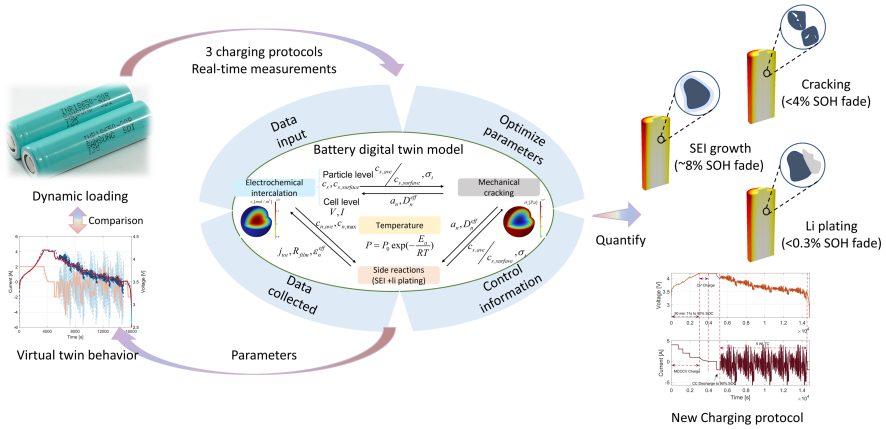


Fig. 3.20: Overview of NMC battery aging quantification using the digital twin process, highlighting the interactions between various aging mechanisms and offering insights for enhancing cycle life. Source: [J3].

Three charging protocols with dynamic discharging profiles were utilized to simulate real-world vehicle operations [C2]. These measurements, alongside operando impedance measurements and post-mortem analysis, were used to validate the digital twin model [J3]. As shown in Fig. 3.21(a-b), the digital twin predicts battery capacity fade within an accuracy of 0.4% MAE up to 10% degradation. The MAEs for relative R_{SEI} (%) at 1C CCCV, 2C CCCV, and MCCCVC are 7.69%, 10.18%, and 4.78%, respectively (Fig. 3.21(c-e)) [J3]. For relative R_{ct} (%), the MAEs are 5.11%, 2.73%, and 3.59% across the same charging protocols.

3.2. Model Validation

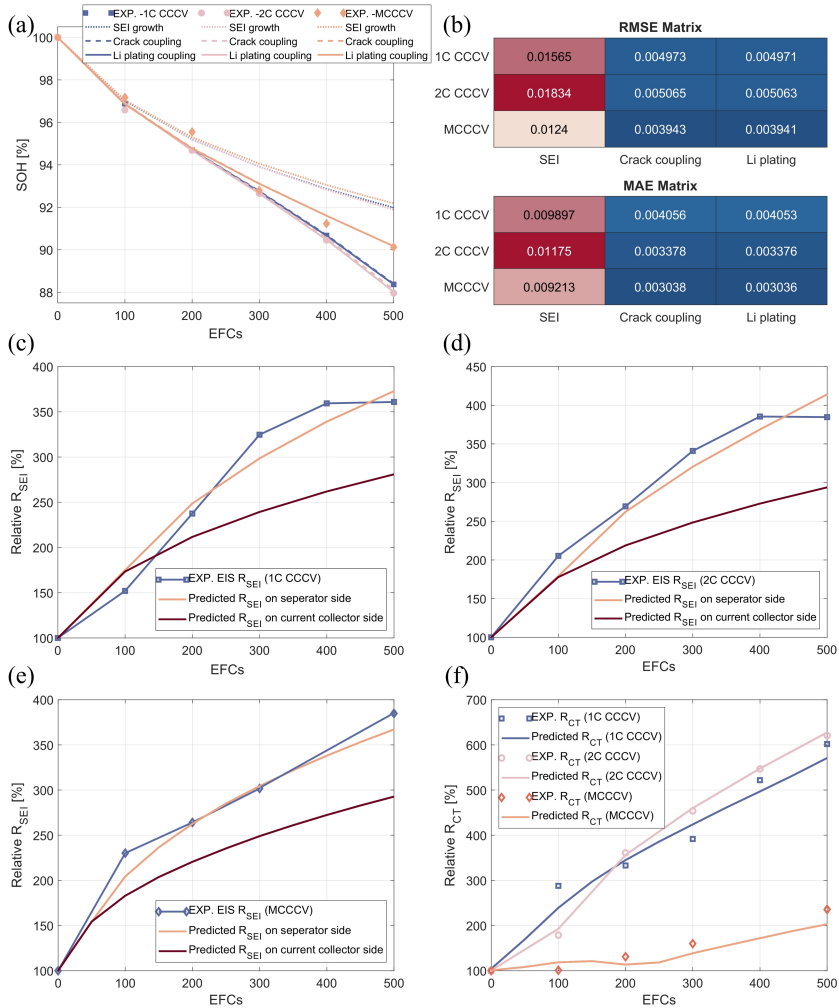


Fig. 3.21: (a) Comparison of predicted and experimental SOH considering the coupling of three mechanisms, (b) digital twin error analysis, and comparison of experimental vs. predicted SEI film resistance at the anode/separator and anode/current collector interfaces for (c) 1C CCCV, (d) 2C CCCV, (e) MCCC. (f) Comparison of experimental and predicted charge transfer resistance increases for the three charging protocols. Source: [J3].

To further validate the model prediction results, this digital twin model were used to predict the degradation behaviors for cells aged until 20% capacity fade. Fig. 3.22 compares the measured and predicted values of capacity, relative R_{SEI} , and R_{ct} , accounting for the coupled effects of SEI growth, electrolyte consumption, lithium plating, and graphite cracking. Panels (a-c) show results under varying fast charging rates at 35°C, (d-f) at 25°C, and (g-i) for different DODs and temperatures. The RMSE and MAE for capacity prediction are

less than 4.5% and 2.7%, indicating high accuracy (Fig. 3.22(j)). The MAE for R_{SEI} and R_{ct} predictions are below 4.4% and 9.3%, respectively, confirming reasonable impedance trend tracking (Fig. 3.22(n-o)).

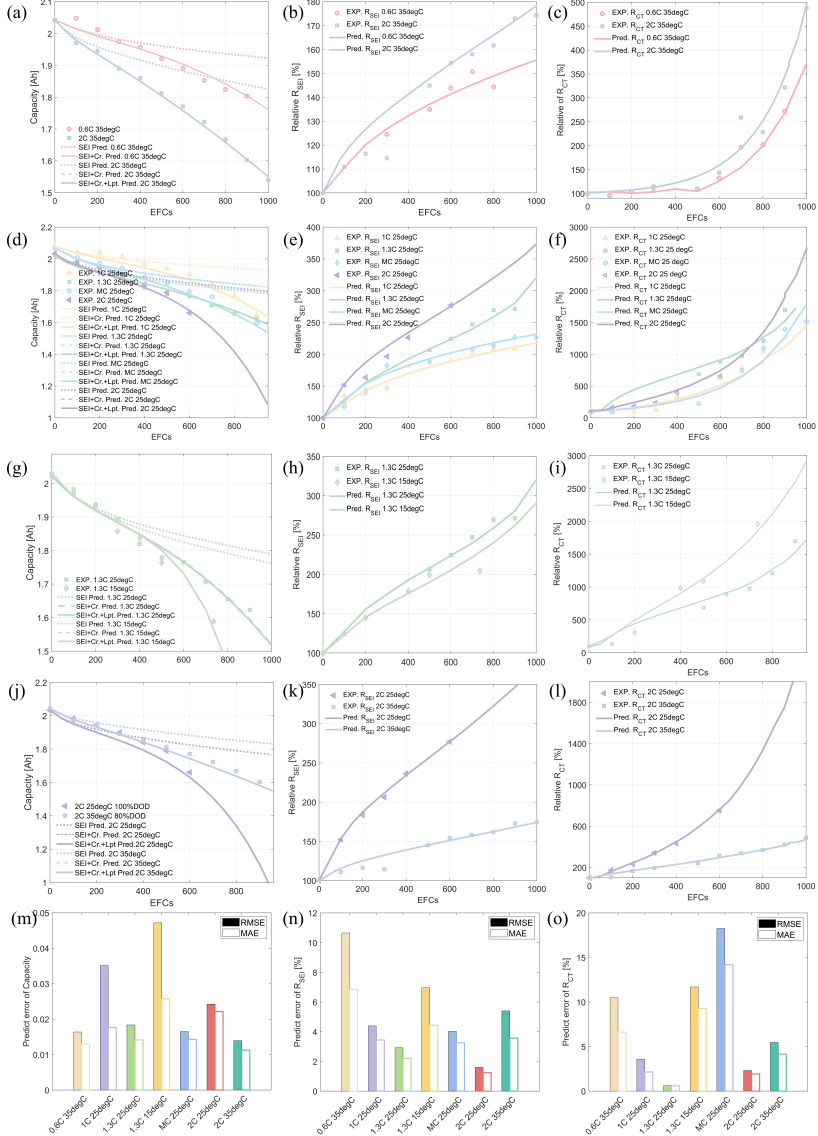


Fig. 3.22: Predicted capacity fade, relative R_{SEI} increase, and R_{ct} growth using the proposed digital twin model at (a-c) 35 °C, (d-f) 25 °C, (g-i) 15 °C, and (j-l) various DODs and temperatures. Subfigures (m-o) display the RMSE and MAE for predicting capacity, R_{SEI} , and R_{ct} under different conditions. Source: supplementary material in [J4].

3.2.2 Aging Mechanisms Quantification

SEI Growth Effect To gain quantitative physical insights, digital twin results reveal that SEI film growth leads to a steady increase in SEI thickness (Fig. 3.23(a)), causing capacity density fade to stabilize into a linear progression. Higher C-rates accelerate SEI growth, with thickness reaching up to several hundred nanometers, consistent with the ranges reported in [47], [48]. Additionally, local anodic porosity decreases after 1000 EFCs, as illustrated in Fig. 3.23(b). Initially at 0.67 in a fresh cell, porosity drops below 0.59 under 2C charging, while less pronounced decreases are observed with 1.3C (below 0.61), MC (below 0.64), and 1C (below 0.65). The MC protocol better prevents pore clogging near the separator compared to the 1.3C protocol. Electrolyte consumption (Fig. 3.23(d)) is directly linked to the SEI reaction rate. The 2C charging protocol shows the most significant reduction in electrolyte volume fraction, followed by 1.3C and MC, with 1C showing the least decline. This indicates that high C-rates accelerate SEI layer formation, though results suggest that C-rates alone are not the primary drivers of accelerated SEI growth.

Crack Formation Effect Fig. 3.23(e) illustrates the tangential stress on graphite particles at the end of constant current (CC) fast charging for the four different charging rates considered. For additional protocols, refer to [J4]. Previous studies [J4] show that the maximum tangential stress occurs at the end of CC charging, reaching approximately 4.4×10^7 Pa at 2C, nearly four times higher than at 1C (1.2×10^7 Pa). In the MC charging protocol, peak tangential stress (2×10^7 Pa) arises at 80% SOC when the charging current transitions from 1C to 0.5C. During delithiation (Fig. 3.23(f)), the maximum tangential stress is lower and has an opposite orientation compared to charging, with the highest stress observed at 2C, followed by 1.3C and 1C. The MC protocol results in the lowest stress, both at the particle center and surface. Repeated cycles of tangential stress at crack sites on graphite contribute to the initiation of fatigue cracks. As depicted in Fig. 3.23(g), crack propagation significantly accelerates capacity loss, especially around 600 EFCs. The 1C and MC fast charging protocols effectively reduce stress levels, thereby slowing crack propagation (Fig. 3.23(g)). After 1000 EFCs, the capacity density fade under the 1.3C, MC, and 1C charging protocols is $8.9 \text{ Ah}/m^2$, $8.1 \text{ Ah}/m^2$, and $7.8 \text{ Ah}/m^2$, respectively, corresponding to 47%, 43%, and 41% of the capacity loss caused by the 2C charging protocol, potentially extending battery life (Fig. 3.23(h)). Post-mortem SEM analysis (Fig. 2.16(a)) supports these findings, showing that the 2C protocol causes more severe graphite cracking and exfoliation, whereas the 1C and MC protocols better preserve the structural integrity of graphite particles.

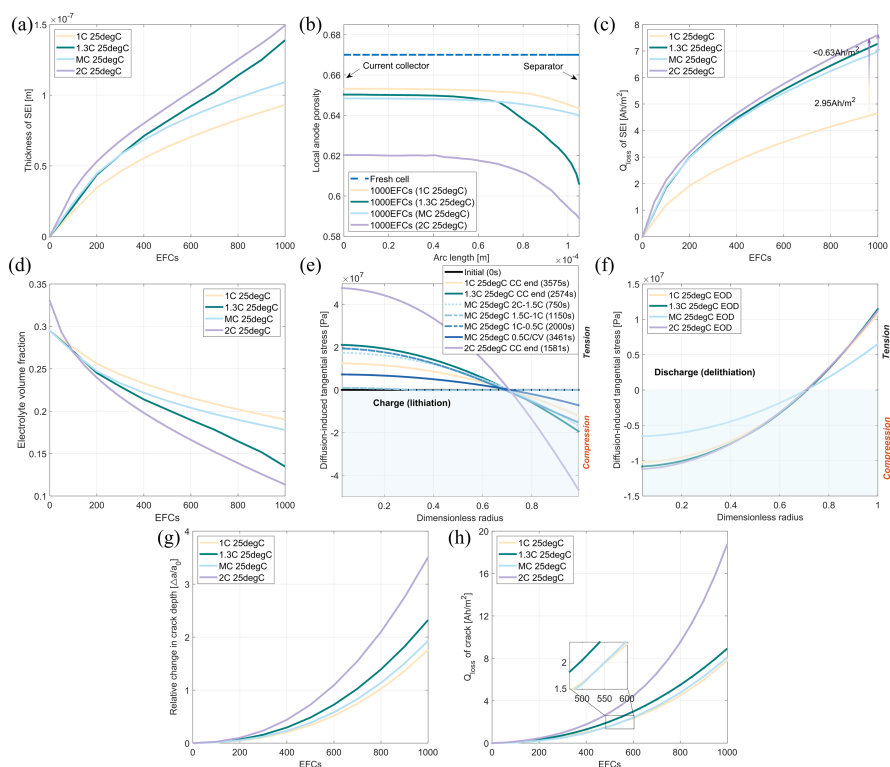


Fig. 3.23: Comparison of digital twin predictions for SEI growth and mechanical behavior at the graphite/separator interface under different aging protocols (1C, 1.3C, MC, and 2C): (a) SEI film thickness; (b) local anode porosity in a fresh cell and after 1000 EFCs; (c) capacity density loss; (d) electrolyte volume reduction; (e) tangential stress distribution within the anode particle at the end of the CC stage; (f) tangential stress at the end of discharge (EOD); (g) crack propagation as a function of EFCs; (h) capacity density loss due to crack growth. Source: [J4].

Lithium Plating Effect Fig. 3.24 illustrates the lithium plating process in cells subjected to four different charging C-rates. For additional protocols, please refer to [J4]. By comparing SOC changes at BOL and after 1000 EFCs, it is evident that the intercalation current shifts towards higher SOC in all cases (Fig. 3.24(a-d)). During aging with the 1C, MC, 1.3C, and 2C protocols, the CC duration decreases to 0.9, 0.8, 0.7, and 0.6 times that at BOL, respectively, while the CV duration extends to 1.5, 2.4, 3.5, and 3.8 times that at BOL. A comparative analysis at 100 EFCs reveals that the intercalation current density at 2C (Fig. 3.24(d)) is roughly ten times higher than at 1C (Fig. 3.24(a)), persisting until the anode potential drops below 0 V. This increased current density can expedite lithium plating, which occurs when the lithium-ion transfer rate from the electrolyte to the anode surpasses the anode’s intercalation capacity, resulting in metallic lithium deposition on the anode surface. After

3.2. Model Validation

1000 EFCs, the intercalation current density for all protocols shifts towards higher SOC, preventing the battery from reaching its initial 0% SOC. Except for the MC protocol, lithium plating exhibits an exponential growth trend (Fig. 3.24(e)), indicating effective suppression under MC fast charging. The findings show that at 25 °C, lithium plating has a negligible impact on capacity fade compared to SEI growth and anode cracking. However, high C-rate charging induces significantly more lithium plating than the MC protocol.

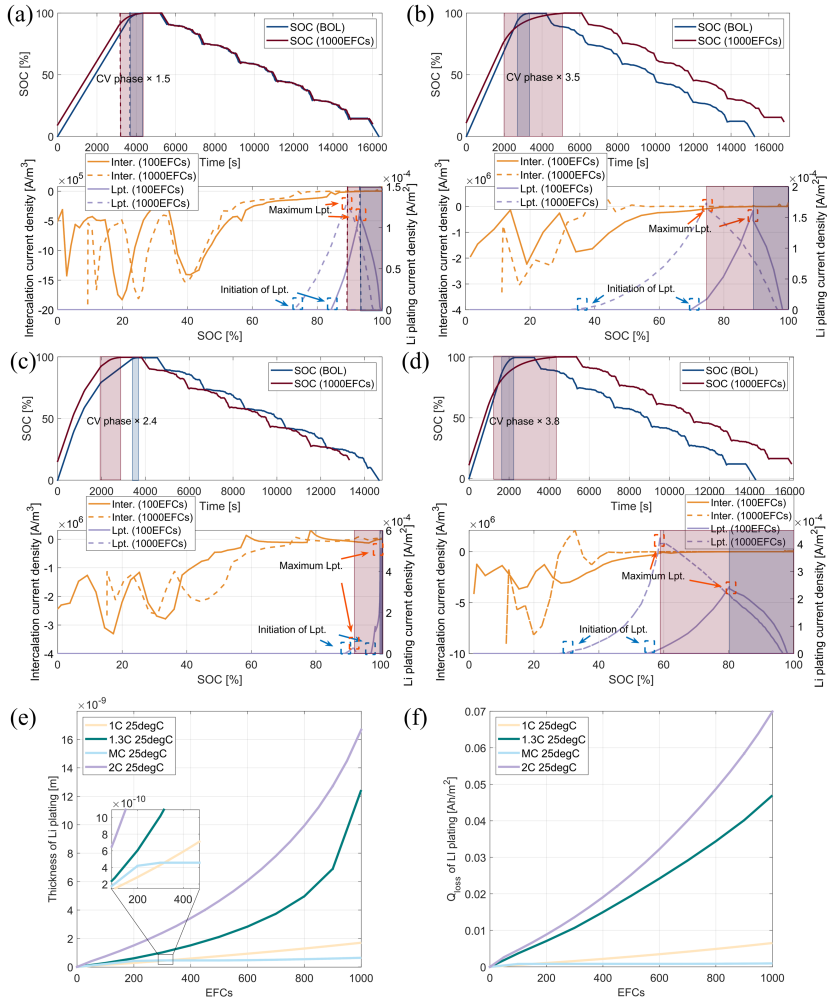


Fig. 3.24: Unraveling lithium plating behavior through digital twin at different charging rates: SOC variations, intercalation current, and lithium plating current density at the anode/seperator interface for (a) 1C, (b) 1.3C, (c) MC, and (d) 2C charging protocols at 100 and 1000 EFCs; (e) Li plating thickness at the anode/seperator interface; (f) capacity density loss attributed to lithium plating. Source: [J4].

3.2.3 Degradation Diagnosis

To quantitatively assess different aging modes under different conditions, we apply the following equations, which take into account the predicted stoichiometry parameters and remaining capacities of both the positive electrode (PE) and negative electrode (NE) [49].

$$LLI = 1 - \frac{Q_{n,EFC}\theta_{EOC,EFC}^- + Q_{p,EFC}\theta_{EOC,EFC}^+}{Q_{n,0}\theta_{EOC,0}^- + Q_{p,0}\theta_{EOC,0}^+} \quad (3.19)$$

$$LAM_p = 1 - \frac{Q_{p,EFC}\theta_{EOD,EFC}^+}{Q_{p,0}\theta_{EOD,0}^+} \quad (3.20)$$

$$LAM_n = 1 - \frac{Q_{n,EFC}\theta_{EOC,EFC}^-}{Q_{n,0}\theta_{EOC,0}^-} \quad (3.21)$$

Diagnostic results across all aging conditions indicate a significant increase in LAM during pronounced aging stages for NMC532 batteries. The difference between LAMneg and LAMpos decreases to just 7.9% after 1000 EFCs. When comparing these findings with the IC peak intensity changes in the full cell pOCV curve, the absolute error (AE) of the digital twin's diagnostics remains within 10% (Fig. 3.25(g)). Likewise, LLI shows a sharp increase in the later aging stages. As shown in Fig. 3.25(h), the AE of LLI diagnostics, compared to DV shift measurements, is within 3.9%, demonstrating the digital twin's diagnostic precision. LLI and LAMneg emerge as the primary aging modes during fast charging, with LAMpos having a lesser impact—this is further validated by post-mortem analysis (Fig. 3.25). These aging mechanisms—LLI, LAMpos, and LAMneg—contribute to the changes in full-cell SOC, explaining the increase in initial 0% SOC observed in sections 3.2.2. This behavior is consistent with the descriptions in [50] regarding the impact of aging modes on full-cell SOC and the adjustments to 100% SOC at the start of each aging cycle.

3.2. Model Validation

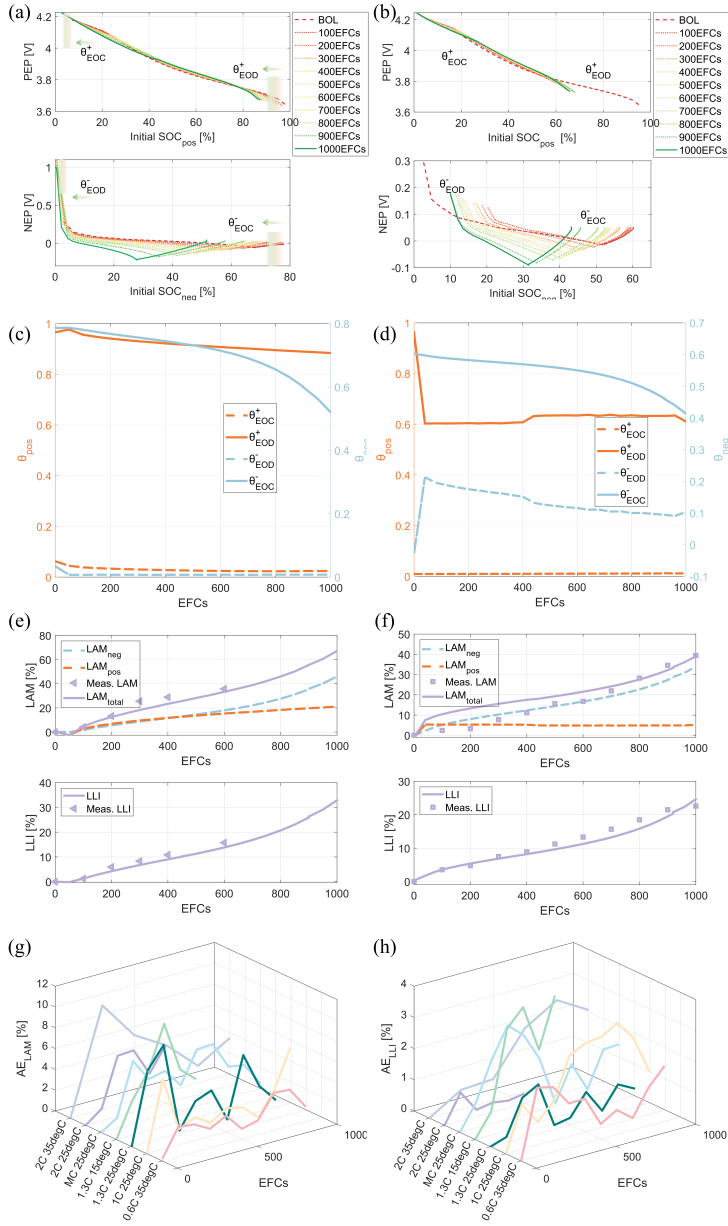


Fig. 3.25: Digital twin diagnostic results for 2C 25°C (100% DOD) and 2C 35°C (70% DOD) scenarios; (a, b) Changes in the negative electrode potential (NEP) and positive electrode potential (PEP) during charging, comparing initial (dashed lines) and aged states (solid lines), with gradient boxes indicating stoichiometry shifts; (c, d) Reduction in stoichiometry ratios at end-of-charge (EOC) and end-of-discharge (EOD) over EFCs; (e, f) Progression of identified aging modes with EFCs; (g, h) Absolute error (AE) in predicted LAM and LLI as a function of EFCs. Source: [J4].

3.3 Summary

This chapter introduces a lithium-ion battery digital twin designed to capture real operational data and model the complex interactions between SEI layer growth, anode crack propagation, and lithium plating. The digital twin estimates aging behavior from the full-cell level down to the particle scale, analyzing voltage-current profiles under varying aging conditions. It provides accurate predictions of NMC-based lithium-ion battery degradation and facilitates detailed electrochemical analysis. An advanced version of the digital twin integrates electrochemical methods with post-mortem analysis to quantify chemical and structural degradation modes. The findings underscore the digital twin's potential for accurately assessing aging effects and provide a robust physics-based framework for developing future physics-informed machine learning model to predict battery degradation.

Chapter 4

Degradation Prediction

Modelling blending ML and Digital Twin Knowledge

This chapter explores the performance of predicting battery health status by combining machine learning with physics-based insights from a digital twin. First, a mixed-input LSTM network is introduced, which integrates partial charging history with operational conditions, serving as a foundational pure machine learning approach for developing a physics-informed method. Next, a Physics-Informed Neural Network (PINN) is developed to predict the capacity loss of lithium-ion batteries. This approach aims to offer more reliable, stable, and accurate capacity predictions by incorporating the battery's dynamic behavior and degradation trends, surpassing traditional neural networks. The related scientific outcomes are as follows:

J5. **W. Guo**, D. I. Stroe, Y. Huang, S. B. Vilsen, Physics-informed machine learning for personalized battery capacity loss prediction, in preparation.

C4. **W. Guo**, Z. Sun, Y. Li, S. Jin, S.B. Vilsen, D.I. Stroe, Health status estimation for lithium-ion batteries with partial charging information using mixed inputs LSTM, 2024 IEEE 10th Int. Power Electron. Motion Control Conf. IPEMC 2024 ECCE Asia. (2024) 1673–1679. <https://doi.org/10.1109/IPEMC-ECCEAsia60879.2024.10567562>.

4.1 Health Status Estimation for Lithium-ion Batteries

4.1.1 Data Description

The dataset contains records of cycling policies, discharge capacity, charging time, and cell temperature. Further details about the dataset are provided in *Chapter 2.2*. The charging protocols employ a multi-stage fast-charging strategy, denoted as C1-C2-C3-C4 [C4]. To account for potential sensor errors or missing data, temperature values were adjusted to align with the set point T . Limited reference performance test (RPT) data was used to create training labels, with additional pseudo-labels created through linear interpolation. A unified model for state-of-health (SOH) estimation under various dynamic aging conditions was developed by combining all aging data without shuffling the time-series labels, yielding 4832 EFCs. The data was split into training, development, and testing sets in a 7.5:2.5 ratio [C4].

4.1.2 Time-series feature extraction

The dQ/dV (IC) curve shows the relationship between capacity and voltage, with the peak's height, position, and area corresponding to the capacity contributions from different voltage plateaus, as described in Eq. 4.22 [C4]. A decrease in the highest peak intensity (3.5V-3.75V) indicates the loss of active materials (LAM), as illustrated in Fig. 4.26(b) [51]. Likewise, the dV/dQ (DV) curve, derived from the differentiation of voltage with respect to capacity (Eq. 4.23), helps quantify the loss of lithium inventory (LLI) [C4], with its endpoint (max Q) acting as a crucial indicator [52].

$$IC = \frac{dQ}{dV} \approx \frac{Q_t - Q_{t-1}}{U_t - U_{t-1}} \quad (4.22)$$

$$dV = \frac{dV}{dQ} \approx \frac{V_t - V_{t-1}}{Q_t - Q_{t-1}} \quad (4.23)$$

4.1. Health Status Estimation for Lithium-ion Batteries

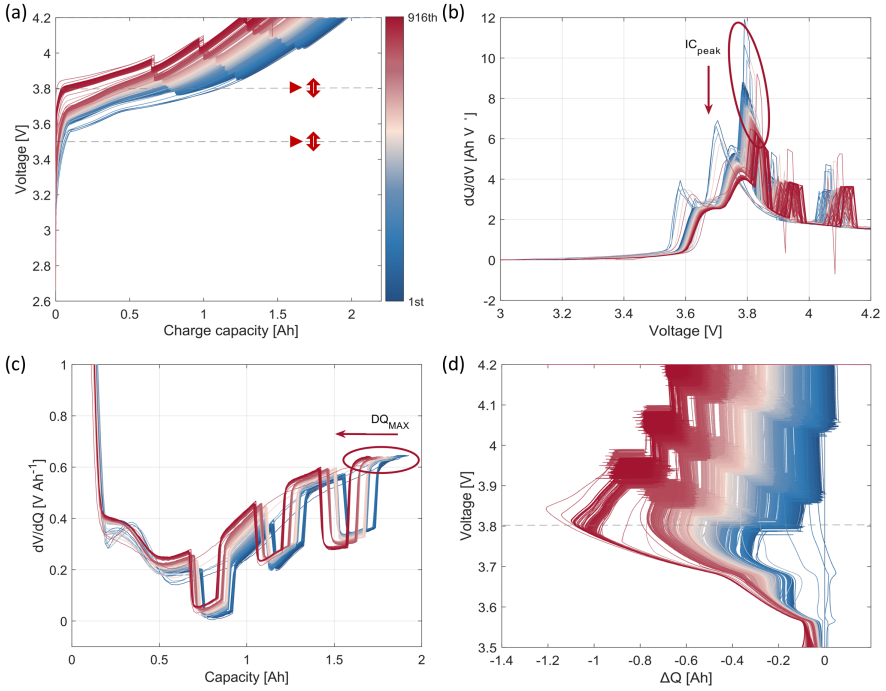


Fig. 4.26: Example of charging curves with partial data selection, showing the difference in charge capacity within the selected range, along with DV and IC curves. The color of each curve represents the battery cycle life, with dark blue indicating BOL and dark red representing EOL. Source: [C4].

Partial $Q - V$ sequences collected during battery charging simulate real-world conditions with incomplete charge cycles (Fig. 4.26(a)). To standardize sequence lengths, linear interpolation is applied. These $Q - V$ sequences, along with cycle-to-cycle differences in voltage (ΔV) and capacity (ΔQ), form the foundation for generating IC and DV curves, and calculating various statistical metrics [53] such as median, minimum, standard deviation, kurtosis, skewness, and Shannon entropy [C4]. Additionally, equivalent full cycles (EFCs) are included. Together, these metrics provide a comprehensive set of health indicators (HIs) for assessing battery health status, as described below.

$$S = \begin{cases} V_s = [V_k, V_{k+1}, \dots, V_l] \\ Q_s = [Q_k, Q_{k+1}, \dots, Q_l] \\ \Delta Q = [\Delta Q_k, \Delta Q_{k+1}, \dots, \Delta Q_l] \end{cases} \quad (4.24)$$

$$HI = [\text{median}(S), \text{min}(S), \text{std}(S), \text{kurt}(S), \text{skew}(S), \text{ShanEn}(S), \text{max}(IC_{peak}), \text{max}(DV_Q), V(IC_{peak}), \text{EOCV}, \text{seq}(CV), \text{EFC}] \quad (4.25)$$

Fig. 4.26 presents the charging IC, DV, and $\Delta Q - V$ (change in charge capacity versus voltage) curves used for feature extraction under the MCCC protocol (details in [3]), with color gradients indicating aging variations (dark blue for BOL to dark red for EOL). This approach has also been consistently applied to other test cases.

4.1.3 Estimation Framework

A deep learning model is utilized for battery SOH estimation, consisting of two LSTM layers followed by a neural network (NN) layer. Given the strong correlation between battery capacity degradation and its operational history [13], the LSTM layers are designed to capture temporal dependencies in the degradation process. The output from the LSTM layers is then combined with two critical aging factors—charging strategies and temperature—and passed into the NN layer. The final output, generated by a single neuron, provides the SOH estimation. This model is designed to accurately predict SOH using partial charging data along with historical information, such as temperature and charging C-rates.

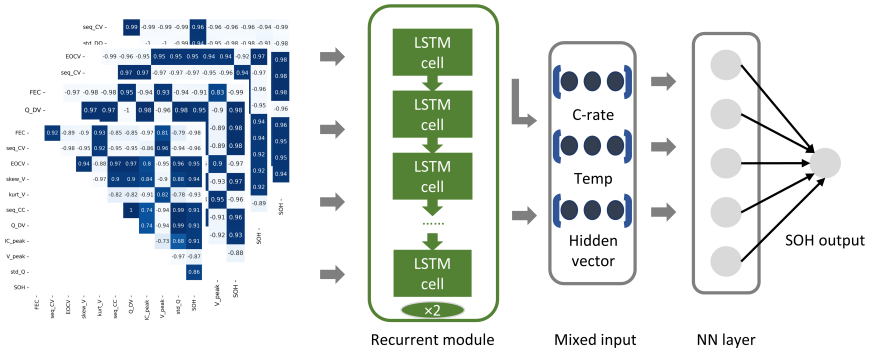


Fig. 4.27: Feature engineering and machine learning framework. The training phase uses a deep learning model that combines recurrent and fully connected layers to uncover the relationships between features and health status. Source: [C4].

4.1.4 Model performance using multi-input LSTM

The estimation framework, depicted in Fig. 4.27, adopts a sequence-to-point method. It takes 10 feature sequences, along with temperature and charging

4.1. Health Status Estimation for Lithium-ion Batteries

C-rates, as inputs and outputs the estimated state of health (SOH). Fig. 4.28 illustrates the SOH estimation results and error distribution, achieving an RMSE of less than 1.54% and an MAE below 1.18%. The model's fitted R^2 value is 0.87, with absolute errors below 0.046, showcasing the framework's robustness for SOH estimation under varying aging conditions using partial charging data.

Additionally, this study compares the proposed method with other machine learning approaches, including linear regression (LR), neural networks (NN), Gaussian process regression (GPR), and support vector machines (SVR). The results are summarized in Table 4.5. Both SVR and GPR use the Radial Basis Function (RBF) kernel, and the hyperparameters for the NN layers are kept consistent with those of the LSTM model. To ensure a fair comparison, training and testing datasets are evaluated without shuffling. Fig. 4.29 presents the test results and SOH estimation errors for each method. While LR produces the smallest error, its overall accuracy is lower compared to the LSTM. In conclusion, the LSTM model surpasses LR, NN, and kernel-based methods in terms of test error and R^2 , demonstrating superior robustness for SOH estimation under various aging conditions using partial charging data.

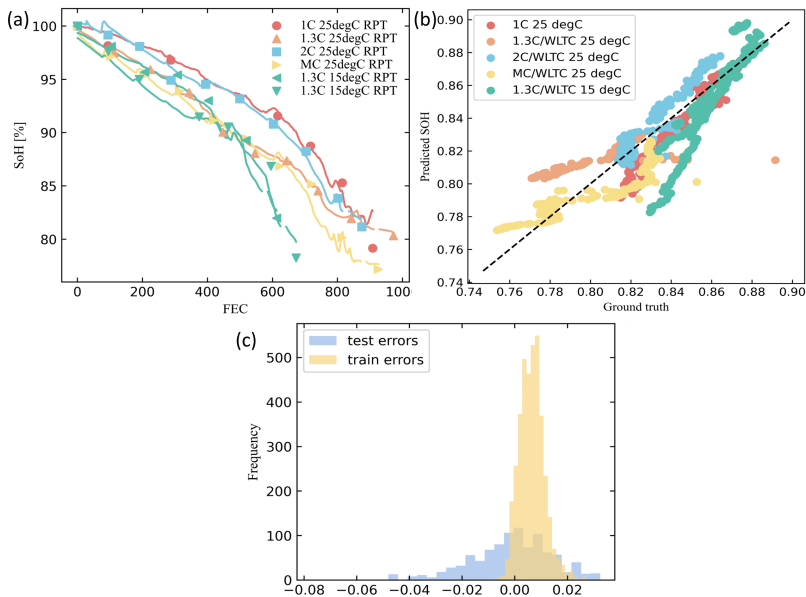


Fig. 4.28: Performance of the mixed-input LSTM: (a) SOH estimation results across six aging protocols, with scatter points showing estimated SOH and the solid line representing actual SOH, (b) Comparison between estimated and actual SOH, and (c) Density distribution of SOH estimation errors. Source: [C4].

Table 4.5: Performance comparison of different methods

Methods	RMSE [%]	MAE [%]	R^2
Mixed-input LSTM	1.54	1.18	0.87
LR	2.44	1.95	0.49
NN	3.21	2.58	0.42
GPR	3.03	2.30	0.21
SVR	2.61	2.08	0.41

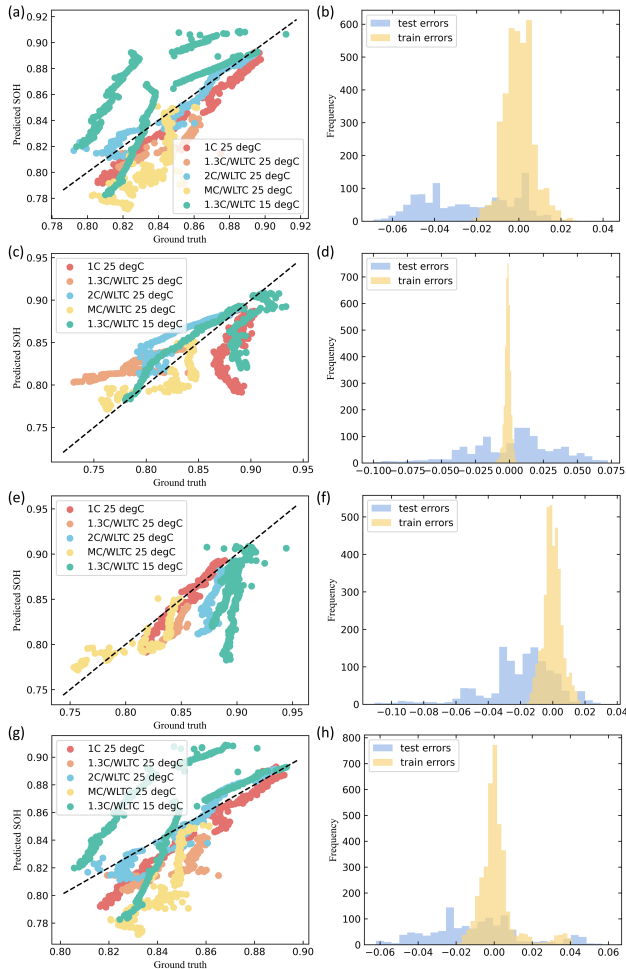


Fig. 4.29: Estimated SOH versus actual SOH for different models: (a) LR, (c) NN, (e) GPR, and (g) SVR; the corresponding density distributions of SOH estimation errors are shown for (b) LR, (d) NN, (f) GPR, and (h) SVR. Source: [C4].

4.2 Physics-informed Machine Learning for Battery Degradation Prediction

4.2.1 Framework overview and flowchart

A Physics-Informed Neural Network (PINN) is developed to predict the capacity loss (Q_{loss}) of lithium-ion batteries, as illustrated in Fig. 4.30. This approach enhances prediction accuracy, stability, and reliability by incorporating the battery's dynamic behavior and degradation trends.

In the data preprocessing stage, statistical features are extracted from the period just before the battery is full charging. This reflects real-world charging conditions, making the method adaptable to various charging and discharging protocols.

In the Q_{loss} prediction stage, integrating electrochemical equations with neural networks (NNs) remains challenging due to the complexity of mechanisms and the numerous highly correlated parameters. In this work, the focus was on modeling battery degradation through crack propagation equations, which were identified as the dominant mechanism from BOL to EOL in the experimented NMC cells, as discussed in *Chapter 3*. This approach allows for the effective integration of governing equations and NNs. The proposed PINN, as shown in Fig. 4.30, consists of two components: a solution function that maps features to Q_{loss} and a nonlinear function Q_{loss} , based on partial differential equations (PDEs) using automatic differentiation. The solution \hat{Q}_{loss} models the relationship between features and Q_{loss} and is expressed as: $Q_{loss}^i = f(\text{EFC}_{\text{norm}}^i, F^i)$, where F^i represents the extracted feature vector, and Q_{loss}^i denotes the capacity loss for the i th EFC. The nonlinear function $Q_{loss}(\cdot)$ models capacity loss based on crack propagation equations. The partial differential equations $\frac{\partial Q_{loss}}{\partial \text{EFC}_{\text{norm}}}, \frac{\partial^2 Q_{loss}}{\partial \text{EFC}_{\text{norm}}^2}$ are influenced by charging rates, particle radius, and material properties. For more details, refer to [J3]. Unknown parameters are determined using ordinary least squares fitted to the training data.

During training, several loss terms are minimized: data loss (L_{data}), monotonicity loss ($L_{monotonicity}$), and physics loss (L_p), as well as PDE constrained losses (L_{PDE1}, L_{PDE2}). These losses reduce errors between predicted and actual values while ensuring the model adheres to the monotonicity and physics-based principles of the degradation model.

To validate the effectiveness of this proposed PINN method, experiments were conducted with small sample sizes (10%, 30%, 50%, and 70% of historical data) in transfer learning scenarios. A standard Feed forward Neural Network (FNN) was used as a benchmark for comparison. In the transfer learning experiments, the parameters and loss terms related to the physical model were frozen while the FNN was fine-tuned on datasets with varying charging pro-

tocols.

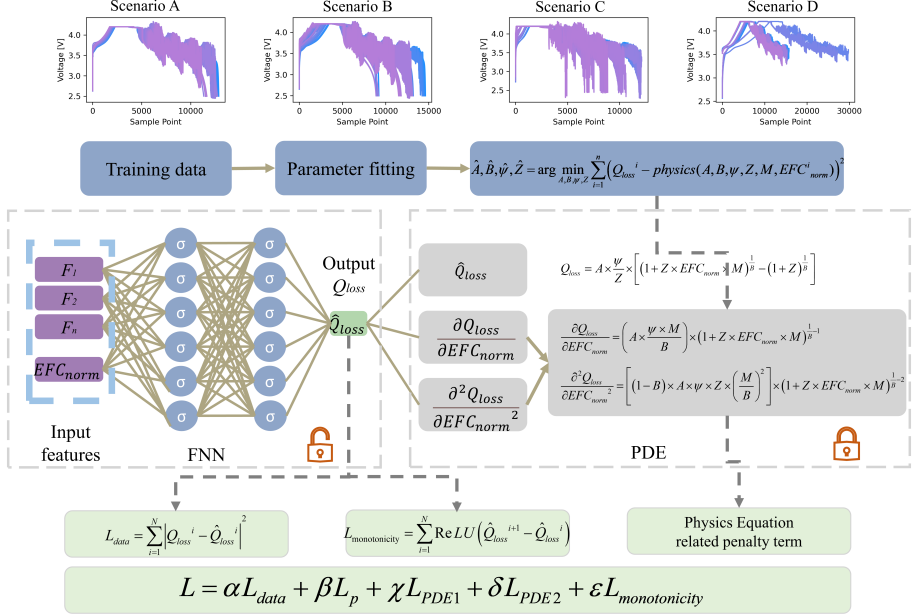


Fig. 4.30: Flowchart of the proposed PINN for predicting lithium-ion battery capacity loss. Different discharge strategies lead to varying degradation trajectories. Features extracted before full charge are used as inputs to predict capacity loss. Q and \hat{Q} represent the true and predicted capacity loss, respectively, with i as the sample index. EFC_{norm} and F_n denote normalized cycles and features, where n is the feature index. The loss function incorporates data, monotonicity, and physics-based terms derived from partial differential equations. Source: [J5].

4.2.2 Feature extraction

Improving capacity prediction performance relies on robust feature extraction, yet identifying generalizable features remains a challenging task. A method is proposed to extract features from a short segment of the charging voltage and current curves, based on observations from multiple charging protocols. Most datasets cover constant current and voltage charging from 3.65V to 4.1V. Regardless of the discharge method or whether the battery is fully discharged (as in scenario D), the charging process is always fully charged. Features were extracted from a short segment of data just before the battery is full charged, as shown in Fig. 4.31. Voltage data between 3.65V and 4.1V was selected, as this range consistently yields reliable results, as demonstrated in [C4]. In particular, the IC peak and DV valley within the 3.65–3.85V range are critical, and these features are also visible in the partial charging curve in Fig. 4.26. For current data, values between 0.5A and 0.1A during the constant voltage phase were used. Regardless of whether the battery was fully discharged, this

4.2. Physics-informed Machine Learning for Battery Degradation Prediction

voltage and current range always appears when the battery is fully charged.

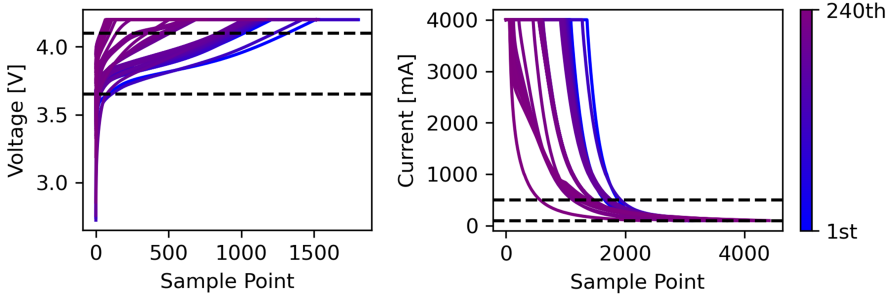


Fig. 4.31: An illustration of the data used for feature extraction, taken shortly before the battery reaches full charge. These features serve as inputs for the proposed PINN model to predict Q_{loss} . They are based on data from 2C/WLTC 0degC, showing how battery aging causes shifts in the voltage and current curves. Source: [J5].

The extracted features include median, kurtosis, skewness, standard deviation, shannon entropy, and curve slope from the selected current, voltage, cumulative charging capacity, and derivatives of capacity curves, along with IC peak height, peak position, DV shift, IC area, end-of-charge voltage, EFC, and the sequence of CC and CV phases (features numbered 1-34). Fig. 4.32 provides an illustration of these features from our experimental dataset, and the Spearman correlation coefficient between the features and capacity loss is calculated, as shown in Fig. 4.33. Unlike other studies (e.g. [54], [55]) that use the Pearson correlation coefficient to evaluate the relationship between features and SOH within the dataset, the spearman correlation is more suitable for capturing nonlinear relationships.

Based on experimental observations and analysis, we found that the correlation coefficient between each feature and capacity loss varies depending on the aging temperature, particularly at low temperatures, and is less influenced by charging/discharging protocols. Additionally, features 3, 6-7, 10-11, 16, and 32-33 show a strong positive correlation with capacity loss, except under the 0°C condition. In contrast, features 1-2, 21-22, 24-25, and 30-31 exhibit a strong negative correlation with capacity loss. Features 15, 19-20 have a weak correlation with Q_{loss} .

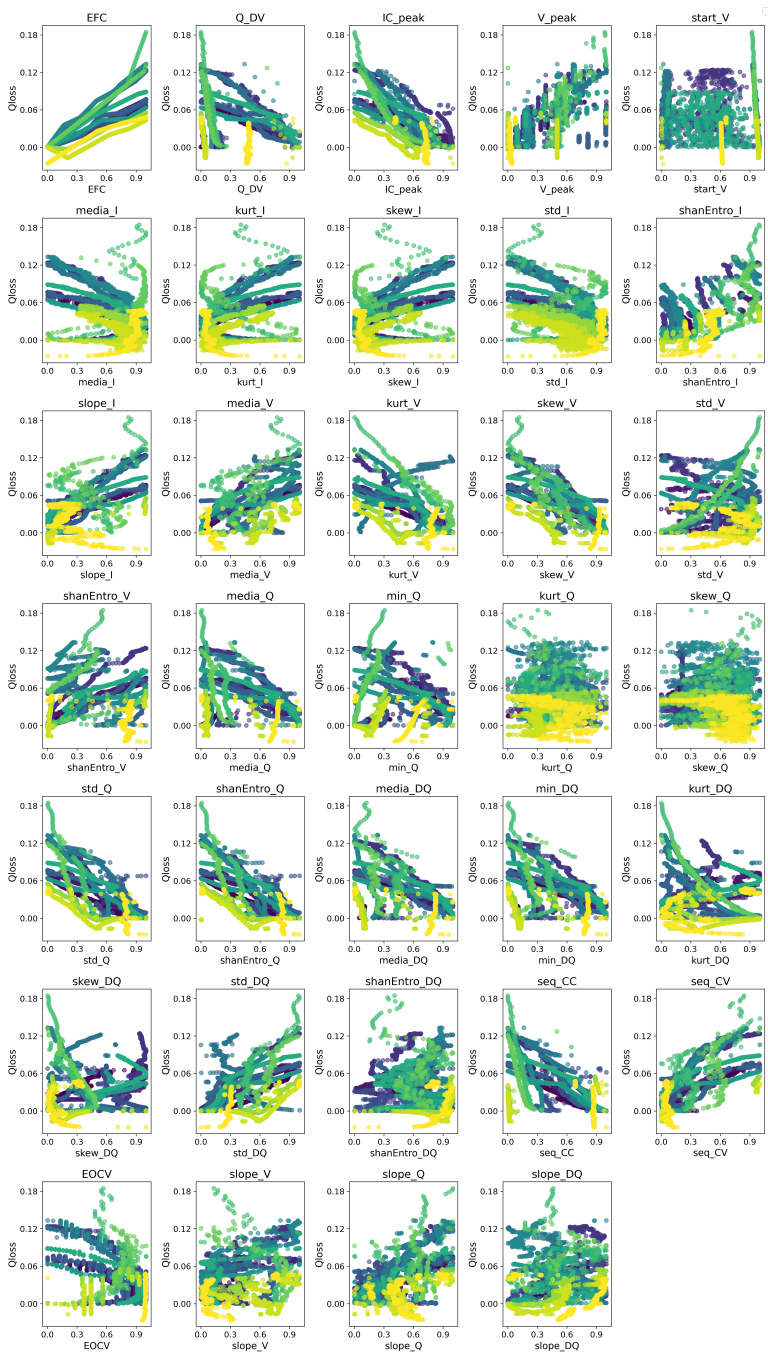


Fig. 4.32: An illustration of the 34 extracted features from 16 batteries in our NMC532 dataset. The x-axis represents Q_{loss} , while the y-axis shows the normalized value of each corresponding feature. Source: [5].

4.2. Physics-informed Machine Learning for Battery Degradation Prediction

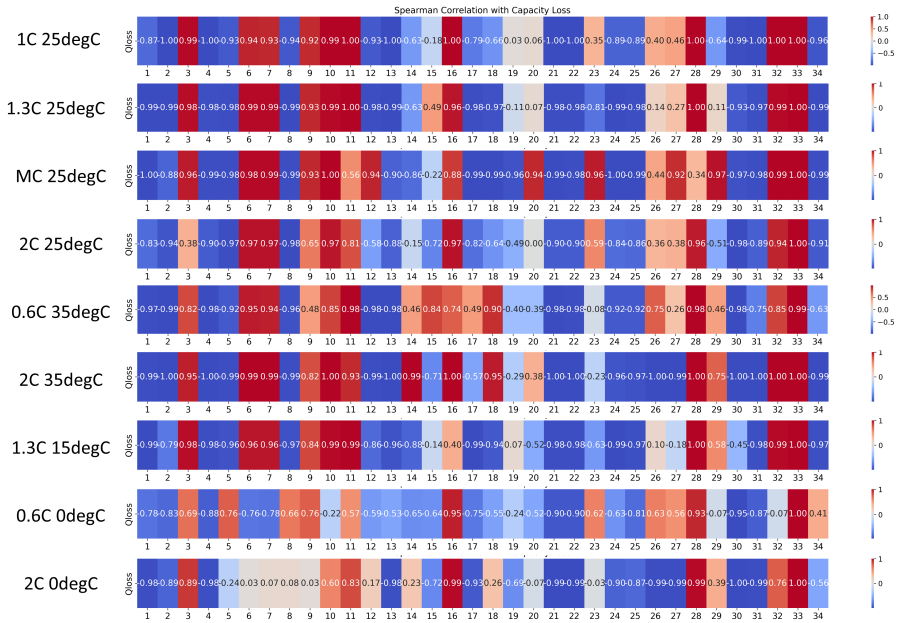


Fig. 4.33: Heatmap showing the correlation between 34 extracted features and Q_{loss} across different aging protocols. The numbers 1-34 correspond to the feature order listed in Fig. 4.32. Source: [J5].

4.2.3 Capacity loss prediction with PINN

The 34 extracted features and time (EFC) serve as inputs for the PINN to predict Q_{loss} ($1 - SOH$). To ensure stability during training and account for varying feature magnitudes, min-max normalization is applied, scaling all features between $[-1, 1]$. The Q_{loss} prediction results for 9 battery cells are shown in Fig. 4.34.

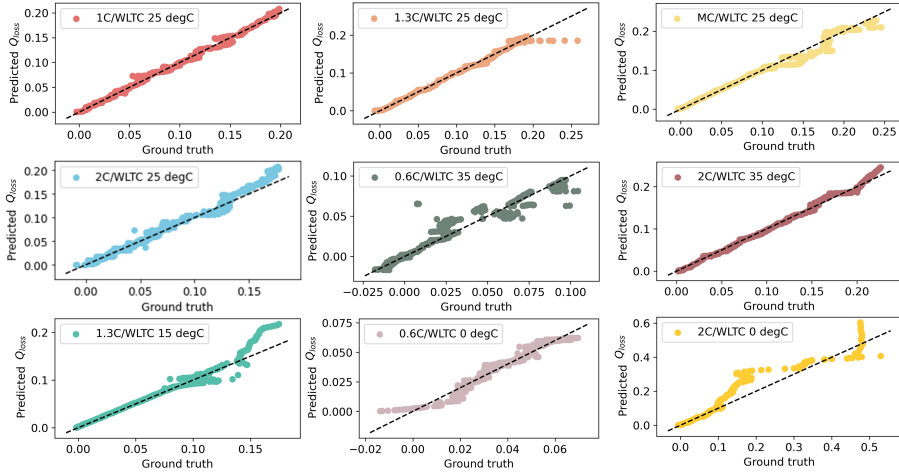


Fig. 4.34: An illustration of capacity loss prediction results. The PINN model is fine-tuned using 50% of the data to predict Q_{loss} for 9 different conditions. Source: [J5].

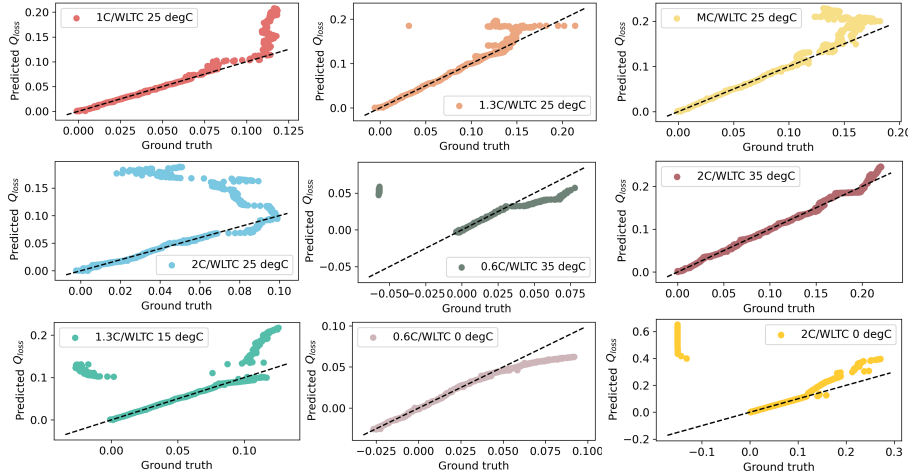


Fig. 4.35: An illustration of capacity loss prediction results using only the benchmark NN model. The NN model is fine-tuned using 50% of the data, resulting in Q_{loss} predictions for 9 different conditions. Source: [J5].

To demonstrate the advancement of the proposed PINN, a conventional neural network (NN) with the same structure and amounts of parameter is used as a benchmark model for comparison. The capacity loss prediction results using the NN are shown in Fig. 4.35. For the 16 battery cells, we select one cell from each protocol (total 7 cells) and split the data into training and validation sets, using 80% for training and 20% for validation. The weight of loss terms in

4.2. Physics-informed Machine Learning for Battery Degradation Prediction

the loss function and weight, bias is saved. Then we use the remaining cells for testing the PINN method. The assumption is that we know the former 50% of historical data, use the saved weight of loss terms, weight, and bias, to retrain the model, and then predict the last 50% of behavior. The results of the 2 models on these 9 test cells are shown in Table 4.6.

The table shows that the proposed PINN outperforms the NN model with lower prediction errors in most cases. The average MAE, MAPE, and RMSE for PINN are 1.6%, 0.11%, and 1.9%, respectively, compared to 6.1%, 0.42%, and 8.3% for the NN model. Notably, both models have identical parameters and structure during inference.

Table 4.6: Comparison of errors between the proposed PINN and NN under different conditions using 50% retraining data.

Condition	Proposed PINN			NN		
	MAE	MAPE [%]	RMSE	MAE	MAPE [%]	RMSE
0.6C/WLTC 0degC	0.004	0.069	0.005	0.023	0.380	0.023
2C/WLTC 0degC	0.064	0.240	0.074	0.170	0.410	0.290
1.3C/WLTC 15degC	0.010	0.047	0.015	0.120	0.880	0.140
1C/WLTC 25degC	0.005	0.046	0.006	0.022	0.150	0.034
1.3C/WLTC 25degC	0.005	0.032	0.008	0.047	0.250	0.052
MC/WLTC 25degC	0.014	0.093	0.016	0.056	0.270	0.062
2C/WLTC 25degC	0.031	0.270	0.031	0.041	0.280	0.064
0.6C/WLTC 35degC	0.009	0.170	0.012	0.062	1.180	0.076
2C/WLTC 35degC	0.005	0.031	0.006	0.008	0.038	0.010

4.2.4 Impact of Data Ratios on Model Prediction Performance

The proposed PINN integrates cracking physical laws to model battery degradation, enabling effective training with less data. Compared to the purely data-driven NN method, the PINN demonstrates better performance, particularly when training data is limited. To confirm this, experiments were carried out using different data ratios to assess its predictive accuracy. The prediction performance for the cells aged under the 1C/WLTC protocol at 25°C is shown in Fig. 4.36.

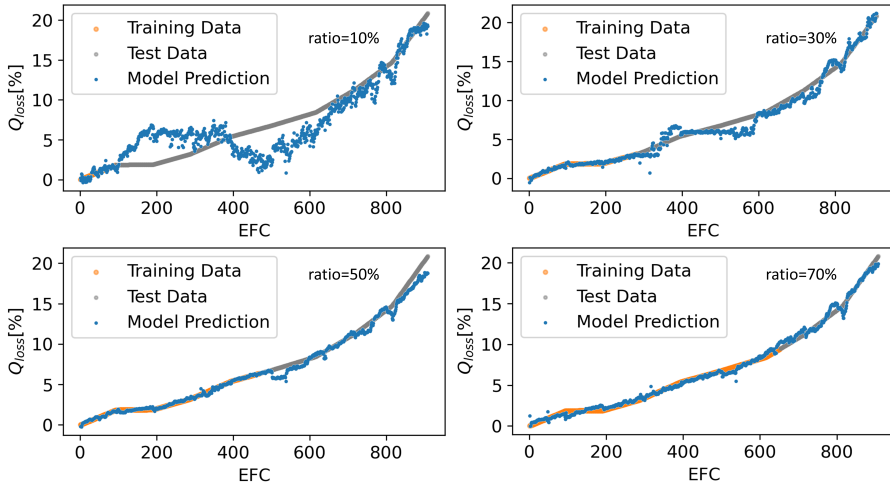


Fig. 4.36: An illustration of Q_{loss} prediction performance using varying data ratios for retraining. Source: [J5].

In each test scenario, data from a single battery cell was split into 80% for training and 20% for validation to train the model. The model was then evaluated on multiple other battery cells. To assess its prediction performance, the model was fine-tuned using varying data ratios (10%, 30%, 50%, and 70%) from the test batteries. The results are presented in Table 4.7 and Fig. 4.37.

It can be observed that the 70% data ratios yield the best results across all tasks. As the retraining data ratio increases, test errors decrease for both models. However, at the 70% data ratio, the MAPE of the PINN model does not narrow as significantly compared to the 30% and 50% ratios. The result still aligns with the common understanding that increasing the number of retraining samples generally enhances model performance when the data is limited. A key conclusion is that, given similar model structures and parameters, the PINN model demonstrates a substantial performance advantage over the NN model in scenarios with limited training data.

4.2. Physics-informed Machine Learning for Battery Degradation Prediction

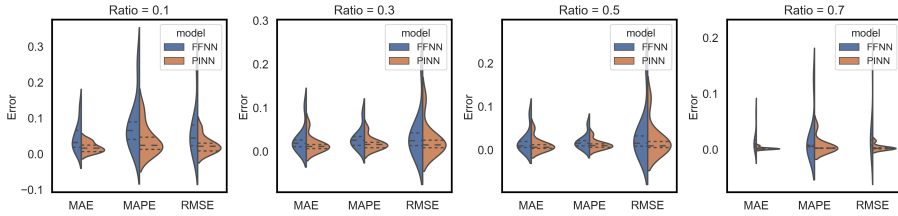


Fig. 4.37: An illustration of Q_{loss} prediction errors for both the proposed PINN and baseline NN models. The graphs depict the distribution of mean absolute error (MAE), mean absolute percentage error (MAPE), and root mean square error (RMSE) across nine conditions, using varying data ratios to retrain the models. Each error bar represents nine experimental points and includes mean and standard deviation markers. The results show that the PINN method achieves lower and more consistent prediction errors compared to the baseline NN. Source: [J5].

Table 4.7: Comparison of average error metrics between the Proposed PINN and NN models retrained with different data ratios. Source: [J5].

Data Ratio	Proposed PINN			NN		
	MAE	MAPE [%]	RMSE	MAE	MAPE [%]	RMSE
10%	0.018	3.901	0.025	0.046	8.410	0.070
30%	0.016	1.803	0.027	0.027	3.015	0.045
50%	0.011	1.177	0.024	0.020	1.901	0.040
70%	0.002	0.680	0.003	0.016	2.030	0.032

4.2.5 Summary

This chapter presents a novel PINN framework designed for predicting degradation behaviors in scenarios with limited data. Initially, a purely machine learning approach, the mixed-input LSTM, was developed to create a unified SOH estimation model. This model combines physics-based health indicators with features extracted from experimented NMC532 dataset, which covers a range of cycling conditions. By using limited RPT data and generating pseudo-labels via linear interpolation, the mixed-input LSTM demonstrated superior performance, achieving RMSE and MAE values below 1.54% and 1.18%, respectively, outperforming traditional methods like LR, NN, GPR, and SVR. Key features, such as changes in peak and valley intensities and positions in IC/DV curves, were extracted from partial charging curves ranging from 3.65V to 4.1V, guided by domain expertise. Building on this foundation, the PINN frame-

work integrates partial differential equations governing crack propagation to optimize neural network parameters. The training process included data loss, monotonicity loss, and physics-based loss terms. Validation on NMC532 cells showed that the PINN model achieved lower prediction errors compared to conventional NN models. Further experiments using different data ratios to retrain the PINN revealed that incorporating physical knowledge significantly improves the learning accuracy of neural network.

Chapter 5

Conclusions and Future Work

This chapter presents the key research findings and contributions from the PhD project, *Physics-Informed Machine Learning for Predicting The Degradation Behavior of Lithium-ion Batteries*. It highlights the main outcomes and discusses potential directions for future research.

5.1 Summary

The main objective of this PhD project was to demonstrate that machine learning and physical insights can work together to create a physics-informed method for improving the accuracy and adaptability of lithium-ion battery degradation predictions. The project focused on developing a battery digital twin model and deriving physical insights from high-fidelity datasets, which encompass various dominant degradation mechanisms while maintaining mechanism consistency for lifetime extrapolation. Dominant degradation mechanisms were then integrated into loss function to constrain the machine learning algorithm, enhancing prediction accuracy with limited historical data. Three technical objectives were addressed in this thesis, and their outcomes are summarized as follows.

The first technical objective was to rank stress factors and identify suitable operational intervals to make effective test plans that accurately simulate realistic cell degradation over a short period while maintaining consistency in aging mechanisms. In *Chapter 2*, three levels of major stress factors were applied over a 43-month calendar aging test and a 10-month cyclic aging test. The evolution of statistical distribution parameters, guided by a consistent acceleration factor, was analyzed to determine mechanistically consistent intervals. The results indicate that for temperature, a range of 35 °C to below 47.5 °C is appropriate for accelerated tests. The impact of SOC levels on calendar aging is minimal; however, for cycling aging, acceptable acceleration occurs below 72.5% SOC. As for CD levels, the aging mechanism remains consistent between 10% and

60%. Based on these findings, a test matrix was designed to simulate various dominant aging mechanisms, providing a dataset for subsequent modeling development.

The second technical objective was to investigate the application of the digital twin concept in predicting battery degradation behavior. In *Chapter 3*, a digital twin model for lithium-ion batteries is proposed, capturing real measurement data and integrating the complex interactions between SEI layer growth, anode crack propagation, and lithium plating. Findings from NMC532 cells, combined with post-mortem analysis, reveal that SEI growth is the primary cause of capacity loss until a 10% capacity fade is reached. As the battery degrades, anode cracking becomes a significant non-linear factor, accelerating degradation. The MC protocol has shown effectiveness in reducing capacity loss due to lithium plating. Operating at a lower depth of discharge also significantly mitigates capacity loss related to anode cracking and SEI growth. After 1000 EFCs, the dominant aging modes in NMC532 cells are loss of active material (LAM) in the negative electrode and loss of lithium inventory (LLI), both of which exceed LAM in the positive electrode. Multistep fast charging, compared to constant current charging, mitigates lithium plating and graphite cracking, resulting in a 13% reduction in LAM. Additionally, optimizing the DOD results in at least a 4% reduction in LLI and a 16% reduction in LAM in the positive electrode. This digital twin model serves as a basis for developing a physics-informed machine learning algorithm to enhance the adaptability of degradation predictions.

The third technical objective was to explore how incorporating physics laws can enhance machine learning performance in small sample scenarios. Initially, a mixed-inputs LSTM is developed to provide unified SOH estimation across various charging/discharging protocols. Domain knowledge is used to extract key features, such as peak and valley intensities and their positions within IC/DV curves, from partial charging data between 3.65V and 4.1V. With limited RPT data for training and additional pseudo-labels generated via linear interpolation, the LSTM achieved RMSE and MAE values below 1.54% and 1.18%, respectively, outperforming other machine learning models such as LR, NN, GPR, and SVR. Next, 34 features along with time (EFC) were used as inputs for the proposed PINN to predict Q_{loss} ($1 - SOH$). The results demonstrated that the PINN achieved lower prediction errors compared to conventional NN models, with average MAE, MAPE, and RMSE values of 1.6%, 0.10%, and 1.9%, respectively, across 9 test cells, compared to 6.1%, 0.42%, and 8.3% for the NN model. Further experiments showed that using only 10% of historical data for retraining resulted in an RMSE of 2.5% across all tasks, highlighting the effectiveness of the PINN in small sample scenarios.

5.2 Main Contributions

The main contributions achieved by this PhD project can be summarized as follows:

- **An overview of the “grey box” lifetime modeling for lithium-ion battery**

This thesis explores various methods for integrating physics-based and data-driven models, providing a comprehensive review of cutting-edge approaches. The trends in related research are illustrated using line graphs and pie charts, highlighting combinations such as data-driven assisted physical models, physics-guided data-driven methods, and their applications. It is found that electrochemical models effectively capture complex aging behavior under diverse conditions, while machine learning, accounting for 78% of all data-driven methods, is well-suited for handling nonlinear performance and addressing gaps in mechanistic understanding. The potential for physics-guided machine learning to drive further innovation is highly promising.

- **Reasonable test plans for detecting battery’s performance to predict their lifetime more accurately are determined based on statistical distribution.**

As a trade-off between efficiency and mechanistic consistency, accelerated degradation testing requires careful selection of stress factors to determine the operational range and the impact of aging-related factors. A novel approach using statistical distributions and the likelihood ratio parametric bootstrap method is proposed to assess mechanistic consistency without relying on costly post-mortem analysis. This method can identify stress points leading to mechanistic changes within the experimental design.

- **An advanced digital twin is proposed to capture real measurement data for quantitative analysis of various aging mechanisms and modes.**

Digital twin concept is firstly applied in lithium-ion battery degradation prediction field. An improved lithium-ion battery digital twin has been developed to capture real measurement data and model the complex interactions between SEI layer growth, electrolyte consumption, anode crack propagation, and lithium plating. This model can estimate aging behavior from the full-cell scale down to the particle level, encompassing voltage-current profiles. It effectively predicts the degradation of NMC532 cells, identifies aging modes, and assists in electrochemical analysis. By improving root cause analysis of cell degradation, the digital twin provides a quantitative understanding of the combined effects

of various aging mechanisms. It demonstrates the potential of electrochemical digital twins for accurate degradation predictions and serves as a foundation for future physics-informed machine learning models.

- **A novel physics informed machine learning algorithm is developed to improve accuracy and adaptability of lithium-ion batteries degradation prediction performance based on limited historical data.**

A PINN model is proposed to predict battery degradation using the cracking propagation equation, as this mechanism was identified as the primary contributor to degradation from BOL to EOL in our NMC532 cells. The auto-differentiation of cracking mechanism equations effectively integrates the loss function with neural networks. The PINN framework includes two main components: a solution function that maps features to Q_{loss} and a nonlinear function Q coupled with partial differential equations through automatic differentiation. The results show that this approach captures battery degradation dynamics more accurately than conventional NN models. The PINN highlights the potential of physics-guided machine learning in modeling battery aging and predicting capacity loss, achieving an average RMSE of less than 0.45% using only 30% of historical data for retraining.

5.3 Future Research Perspectives

This PhD has investigated the modelling of degradation mechanisms of NMC/Graphite lithium-ion batteries, digital twin concept in LiBs degradation prediction field, and physics-informed neural network to improve the accuracy and adaptability based on limited data. There are still challenges to develop a real-time digital twin and choose reasonable physical insights to obtain a much feasible PINN algorithm. Several aspects for further studies are summarized as follows.

- **Lithium plating mechanism at 0°C requires further calibration.**
The digital twin model has been validated with data collected at 15°C, 25°C, and 35°C. Additional parameter estimation and performance testing should be conducted and validated using data at 0°C.
- **Cathode degradation mechanisms should be considered to improve the digital twin model.**
The digital twin model incorporates the strongly coupled effects of dual-layer SEI growth, lithium plating, and anode particle crack propagation. Currently, it does not account for cathode particle cracking, as minimal cracking was observed after aging. However, cathode mechanisms, such as transition metal dissolution, could be included in future modeling efforts.

5.3. Future Research Perspectives

- **A real-time digital twin needs to be further developed.**
Currently, profile data must be loaded directly to achieve the twin perception component, and four sensitive parameters need to be estimated at BOL. Next, three aging parameters are fitted for the first 200 EFCs to obtain prediction results. Running this process in real-time using COMSOL Multiphysics with Matlab is challenging due to computational constraints, although parallel execution with new data is possible. Future work should focus on developing a simulation App that requires less hardware and can provide faster results.
- **The proposed PINN model needs to be validated on other chemistries.**
The proposed PINN model was validated by transferring physical degradation knowledge from different test conditions to the remaining cells using a transfer strategy. Its prediction performance was assessed using our own dataset of 18 NMC532 battery cells. To further demonstrate the model's superiority and versatility, additional datasets with different chemical compositions and charge/discharge protocols should be considered.
- **Another PINN strategy, using physical information embedded in features, will be explored to determine if it can improve prediction performance.**
Another potential PINN strategy involves generating battery behavior by varying underlying physical parameters and establishing a mapping between real measurement data and these parameters. These physical parameters can then be integrated with extracted features to evaluate whether they improve capacity loss predictions. This strategy warrants further investigation to determine its effectiveness.

References

- [1] S. Vazquez, S. M. Lukic, E. Galvan, L. G. Franquelo, and J. M. Carrasco, "Energy storage systems for transport and grid applications," *IEEE Transactions on Industrial Electronics*, vol. 57, no. 12, pp. 3881–3895, 2010.
- [2] The U.S. Consumer Product Safety Commission, "Amazon Recalls Portable Power Banks Due to Fire and Chemical Burn Hazards (Recall Alert)," 2018. [Online]. Available: <https://www.cpsc.gov/Recalls/2018/Amazon-Recalls-Portable-Power-Banks-Due-to-Fire-and-Chemical-Burn-Hazards-Recall>
- [3] D. I. Stroe, M. Swierczynski, A. I. Stan, R. Teodorescu, and S. J. Andreasen, "Accelerated lifetime testing methodology for lifetime estimation of lithium-ion batteries used in augmented wind power plants," *IEEE Transactions on Industry Applications*, vol. 50, no. 6, pp. 4006–4017, 2014.
- [4] E. Sarasketa-Zabala, I. Gandiaga, L. M. Rodriguez-Martinez, and I. Villarreal, "Calendar ageing analysis of a LiFePO₄/graphite cell with dynamic model validations: Towards realistic lifetime predictions," *Journal of Power Sources*, vol. 272, pp. 45–57, 2014. [Online]. Available: <http://dx.doi.org/10.1016/j.jpowsour.2014.08.051>
- [5] M. Ecker, J. B. Gerschler, J. Vogel, S. Käbitz, F. Hust, P. Dechent, and D. U. Sauer, "Development of a lifetime prediction model for lithium-ion batteries based on extended accelerated aging test data," *Journal of Power Sources*, vol. 215, pp. 248–257, 2012.
- [6] M. Song and S. Y. Choe, "Parameter sensitivity analysis of a reduced-order electrochemical-thermal model for heat generation rate of lithium-ion batteries," *Applied Energy*, vol. 305, no. October 2021, p. 117920, 2022. [Online]. Available: <https://doi.org/10.1016/j.apenergy.2021.117920>
- [7] Z. Khalik, M. C. Donkers, J. Sturm, and H. J. Bergveld, "Parameter estimation of the Doyle–Fuller–Newman model for Lithium-ion batteries by parameter normalization, grouping, and sensitivity analysis," *Journal of Power Sources*, vol. 499, no. January, p. 229901, 2021. [Online]. Available: <https://doi.org/10.1016/j.jpowsour.2021.229901>
- [8] M. Tan, Y. Gan, J. Liang, L. He, Y. Li, S. Song, and Y. Shi, "Effect of initial temperature on electrochemical and thermal characteristics of a lithium-ion battery during charging process," *Applied Thermal Engineering*, vol. 177, no. May, p. 115500, 2020. [Online]. Available: <https://doi.org/10.1016/j.applthermaleng.2020.115500>

References

- [9] G. Jiang, L. Zhuang, Q. Hu, Z. Liu, and J. Huang, "An investigation of heat transfer and capacity fade in a prismatic Li-ion battery based on an electrochemical-thermal coupling model," *Applied Thermal Engineering*, vol. 171, no. September 2019, p. 115080, 2020. [Online]. Available: <https://doi.org/10.1016/j.applthermaleng.2020.115080>
- [10] M. K. Tran, A. Mevawala, S. Panchal, K. Raahemifar, M. Fowler, and R. Fraser, "Effect of integrating the hysteresis component to the equivalent circuit model of Lithium-ion battery for dynamic and non-dynamic applications," *Journal of Energy Storage*, vol. 32, no. May, p. 101785, 2020. [Online]. Available: <https://doi.org/10.1016/j.est.2020.101785>
- [11] H. Mu and R. Xiong, "Modeling, Evaluation, and State Estimation for Batteries," in *Modeling, Dynamics and Control of Electrified Vehicles*, H. Zhang, D. Cao, and H. Du, Eds. Duxford: Woodhead Publishing, 2018, ch. 1, pp. 1–38. [Online]. Available: <http://dx.doi.org/10.1016/B978-0-12-812786-5.00001-X>
- [12] D. Chen, L. Xiao, W. Yan, and Y. Guo, "A novel hybrid equivalent circuit model for lithium-ion battery considering nonlinear capacity effects," *Energy Reports*, vol. 7, pp. 320–329, 2021. [Online]. Available: <https://doi.org/10.1016/j.egy.2021.06.051>
- [13] Y. Liu, K. Xie, Y. Pan, H. Wang, Y. Li, and C. Zheng, "Simplified modeling and parameter estimation to predict calendar life of Li-ion batteries," *Solid State Ionics*, vol. 320, no. September 2017, pp. 126–131, 2018. [Online]. Available: <https://doi.org/10.1016/j.ssi.2018.02.038>
- [14] M. Naumann, F. Spingler, and A. Jossen, "Analysis and modeling of cycle aging of a commercial LiFePO₄/graphite cell," *Journal of Power Sources*, vol. 451, no. September 2019, p. 227666, 2020. [Online]. Available: <https://doi.org/10.1016/j.jpowsour.2019.227666>
- [15] L. Ren, G. Zhu, J. Kang, J. V. Wang, B. Luo, C. Chen, and K. Xiang, "An algorithm for state of charge estimation based on a single-particle model," *Journal of Energy Storage*, vol. 39, no. April, p. 102644, 2021. [Online]. Available: <https://doi.org/10.1016/j.est.2021.102644>
- [16] Y. Zheng, W. Gao, X. Han, M. Ouyang, L. Lu, and D. Guo, "An accurate parameters extraction method for a novel on-board battery model considering electrochemical properties," *Journal of Energy Storage*, vol. 24, no. December 2018, p. 100745, 2019. [Online]. Available: <https://doi.org/10.1016/j.est.2019.04.019>
- [17] J. Wang, P. Liu, J. Hicks-Garner, E. Sherman, S. Soukiazian, M. Verbrugge, H. Tataria, J. Musser, and P. Finamore, "Cycle-life model for graphite-

References

- LiFePO₄ cells," *Journal of Power Sources*, vol. 196, no. 8, pp. 3942–3948, 2011. [Online]. Available: <http://dx.doi.org/10.1016/j.jpowsour.2010.11.134>
- [18] G. E. Karniadakis, I. G. Kevrekidis, L. Lu, P. Perdikaris, S. Wang, and L. Yang, "Physics-informed machine learning," *Nature Reviews Physics*, vol. 3, no. 6, pp. 422–440, 2021.
- [19] S. Xu, K.-H. Chen, N. P. Dasgupta, J. B. Siegel, and A. G. Stefanopoulou, "Evolution of Dead Lithium Growth in Lithium Metal Batteries: Experimentally Validated Model of the Apparent Capacity Loss," *Journal of The Electrochemical Society*, vol. 166, no. 14, pp. A3456–A3463, 2019.
- [20] D. Vidal, C. Leys, B. Mathieu, N. Guillet, V. Vidal, D. Borschneck, P. Chau-rand, S. Genies, E. De Vito, M. Tulodziecki, and W. Porcher, "Si-C/G based anode swelling and porosity evolution in 18650 casing and in pouch cell," *Journal of Power Sources*, vol. 514, no. May, 2021.
- [21] M. Kassem and C. Delacourt, "Postmortem analysis of calendar-aged graphite/LiFePO₄ cells," *Journal of Power Sources*, vol. 235, pp. 159–171, 2013.
- [22] E. Prada, D. Di Domenico, Y. Creff, J. Bernard, V. Sauvant-Moynot, and F. Huet, "Simplified Electrochemical and Thermal Model of LiFePO₄-Graphite Li-Ion Batteries for Fast Charge Applications," *Journal of The Electrochemical Society*, vol. 159, no. 9, pp. A1508–A1519, 2012.
- [23] N. Wolff, N. Harting, M. Heinrich, F. Röder, and U. Krewer, "Nonlinear Frequency Response Analysis on Lithium-Ion Batteries: A Model-Based Assessment," *Electrochimica Acta*, vol. 260, pp. 614–622, 2018.
- [24] S. Tippmann, D. Walper, L. Balboa, B. Spier, and W. G. Bessler, "Low-temperature charging of lithium-ion cells part I: Electrochemical modeling and experimental investigation of degradation behavior," *Journal of Power Sources*, vol. 252, pp. 305–316, 2014. [Online]. Available: <http://dx.doi.org/10.1016/j.jpowsour.2013.12.022>
- [25] R. Deshpande, M. Verbrugge, Y.-T. Cheng, J. Wang, and P. Liu, "Battery Cycle Life Prediction with Coupled Chemical Degradation and Fatigue Mechanics," *Journal of The Electrochemical Society*, vol. 159, no. 10, pp. A1730–A1738, 2012.
- [26] J. Li, K. Adewuyi, N. Lotfi, R. G. Landers, and J. Park, "A single particle model with chemical/mechanical degradation physics for lithium ion battery State of Health (SOH) estimation," *Applied Energy*, vol. 212, no. July 2017, pp. 1178–1190, 2018.

References

- [27] M. E. Orazem and B. Tribollet, *Electrochemical Impedance Spectroscopy*. Hoboken: John Wiley Sons, 2008.
- [28] A. Leonide, V. Sonn, A. Weber, and E. Ivers-Tifféé, "Evaluation and Modeling of the Cell Resistance in Anode-Supported Solid Oxide Fuel Cells," *Journal of The Electrochemical Society*, vol. 155, no. 1, p. B36, 2008. [Online]. Available: <https://doi.org/10.1149/1.2801372>
- [29] J. Illig, "Physically based impedance modelling of lithium-ion cells," Ph.D. dissertation, Karlsruhe Institute of Technology, 2014.
- [30] X. Hu, S. Li, and H. Peng, "A comparative study of equivalent circuit models for Li-ion batteries," *Journal of Power Sources*, vol. 198, pp. 359–367, 2012.
- [31] J. Belt, V. Utgikar, and I. Bloom, "Calendar and PHEV cycle life aging of high-energy, lithium-ion cells containing blended spinel and layered-oxide cathodes," *Journal of Power Sources*, vol. 196, no. 23, pp. 10 213–10 221, 2011. [Online]. Available: <http://dx.doi.org/10.1016/j.jpowsour.2011.08.067>
- [32] K. Takei, K. Kumai, Y. Kobayashi, H. Miyashiro, N. Terada, T. Iwahori, and T. Tanaka, "Cycle life estimation of lithium secondary battery by extrapolation method and accelerated aging test," *Journal of Power Sources*, vol. 97-98, pp. 697–701, 2001.
- [33] M. Petit, E. Prada, and V. Sauvant-Moynot, "Development of an empirical aging model for Li-ion batteries and application to assess the impact of Vehicle-to-Grid strategies on battery lifetime," *Applied Energy*, vol. 172, pp. 398–407, 2016. [Online]. Available: <http://dx.doi.org/10.1016/j.apenergy.2016.03.119>
- [34] W. B. Nelson, *Accelerated Testing Statistical Models, Test Plans, and Data Analysis*. John Wiley & Sons, 2004.
- [35] W. Q. Meeker, L. A. Escobar, and C. J. Lu, "Accelerated Degradation Tests: Modeling and Analysis," *Technometrics*, vol. 40, no. 2, pp. 89–99, 1998.
- [36] D. Stroe, "Lifetime models for lithium-ion batteries used in virtual power plant applications," Nov. 2014.
- [37] S. Sun, T. Guan, B. Shen, K. Leng, Y. Gao, X. Cheng, and G. Yin, "Changes of Degradation Mechanisms of LiFePO₄/Graphite Batteries Cycled at Different Ambient Temperatures," *Electrochimica Acta*, vol. 237, pp. 248–258, 2017.

References

- [38] W. Guo, Y. Li, Z. Sun, B. Vilsen, and D. Ioan, "A digital twin to quantitatively understand aging mechanisms coupled effects of NMC battery using dynamic aging profiles," *Energy Storage Materials*, vol. 63, no. September, 2023.
- [39] J. Guo, Y. Li, J. Meng, K. Pedersen, L. Gurevich, and D. I. Stroe, "Understanding the mechanism of capacity increase during early cycling of commercial NMC/graphite lithium-ion batteries," *Journal of Energy Chemistry*, vol. 74, pp. 34–44, 2022. [Online]. Available: <https://doi.org/10.1016/j.jechem.2022.07.005>
- [40] H. Koshikawa, S. Matsuda, K. Kamiya, M. Miyayama, Y. Kubo, K. Uosaki, K. Hashimoto, and S. Nakanishi, "Dynamic changes in charge-transfer resistance at Li metal/Li₇La₃Zr₂O₁₂ interfaces during electrochemical Li dissolution/deposition cycles," *Journal of Power Sources*, vol. 376, no. December 2017, pp. 147–151, 2018. [Online]. Available: <https://doi.org/10.1016/j.jpowsour.2017.11.082>
- [41] K. Dong, Y. Xu, J. Tan, M. Osenberg, F. Sun, Z. Kochovski, D. T. Pham, S. Mei, A. Hilger, E. Ryan, Y. Lu, J. Banhart, and I. Manke, "Unravelling the Mechanism of Lithium Nucleation and Growth and the Interaction with the Solid Electrolyte Interface," *ACS Energy Letters*, vol. 6, no. 5, pp. 1719–1728, 2021.
- [42] R. Pathak, K. Chen, A. Gurung, K. M. Reza, B. Bahrami, J. Pokharel, A. Baniya, W. He, F. Wu, Y. Zhou, K. Xu, and Q. Q. Qiao, "Fluorinated hybrid solid-electrolyte-interphase for dendrite-free lithium deposition," *Nature Communications*, vol. 11, no. 1, pp. 1–10, 2020. [Online]. Available: <http://dx.doi.org/10.1038/s41467-019-13774-2>
- [43] S. J. An, J. Li, C. Daniel, D. Mohanty, S. Nagpure, and D. L. Wood, "The state of understanding of the lithium-ion-battery graphite solid electrolyte interphase (SEI) and its relationship to formation cycling," *Carbon*, vol. 105, pp. 52–76, 2016. [Online]. Available: <http://dx.doi.org/10.1016/j.carbon.2016.04.008>
- [44] H. Ekström and G. Lindbergh, "A Model for Predicting Capacity Fade due to SEI Formation in a Commercial Graphite/LiFePO₄ Cell," *Journal of The Electrochemical Society*, vol. 162, no. 6, pp. A1003–A1007, 2015.
- [45] P. Barai, K. Smith, C.-F. Chen, G.-H. Kim, and P. P. Mukherjee, "Reduced Order Modeling of Mechanical Degradation Induced Performance Decay in Lithium-Ion Battery Porous Electrodes," *Journal of The Electrochemical Society*, vol. 162, no. 9, pp. A1751–A1771, 2015.

References

- [46] W. Li, D. Cao, D. Jöst, F. Ringbeck, M. Kuipers, F. Frie, and D. U. Sauer, "Parameter sensitivity analysis of electrochemical model-based battery management systems for lithium-ion batteries," *Applied Energy*, vol. 269, no. February, p. 115104, 2020. [Online]. Available: <https://doi.org/10.1016/j.apenergy.2020.115104>
- [47] G. Qian, Y. Li, H. Chen, L. Xie, T. Liu, N. Yang, Y. Song, C. Lin, J. Cheng, N. Nakashima, M. Zhang, Z. Li, W. Zhao, X. Yang, H. Lin, X. Lu, L. Yang, H. Li, K. Amine, L. Chen, and F. Pan, "Revealing the aging process of solid electrolyte interphase on SiO_x anode," *Nature Communications*, vol. 14, no. 1, pp. 1–9, 2023.
- [48] J. Guo, Y. Xu, M. Exner, X. Huang, Y. Li, Y. Liu, H. Wang, J. Kowal, Q. Zhang, P. K. Kristensen, D. Wang, K. Pedersen, L. Gurevich, D. I. Stroe, and P. Adelhelm, "Unravelling the Mechanism of Pulse Current Charging for Enhancing the Stability of Commercial LiNi_{0.5}Mn_{0.3}Co_{0.2}O₂/Graphite Lithium-Ion Batteries," *Advanced Energy Materials*, vol. 2400190, pp. 1–14, 2024.
- [49] W. Li, J. Chen, K. Quade, D. Luder, J. Gong, and D. U. Sauer, "Battery degradation diagnosis with field data, impedance-based modeling and artificial intelligence," *Energy Storage Materials*, vol. 53, no. August, pp. 391–403, 2022.
- [50] M. Dubarry, A. Devie, and B. Y. Liaw, "The Value of Battery Diagnostics and Prognostics," *J. Energy Power Sources*, vol. 1, no. 5, pp. 242–249, 2014. [Online]. Available: www.ethanpublishing.com
- [51] P. Verma, P. Maire, and P. Novák, "A review of the features and analyses of the solid electrolyte interphase in Li-ion batteries," *Electrochimica Acta*, vol. 55, no. 22, pp. 6332–6341, 2010. [Online]. Available: <http://dx.doi.org/10.1016/j.electacta.2010.05.072>
- [52] A. Barai, K. Uddin, M. Dubarry, L. Somerville, A. McGordon, P. Jennings, and I. Bloom, "A comparison of methodologies for the non-invasive characterisation of commercial Li-ion cells," *Progress in Energy and Combustion Science*, vol. 72, pp. 1–31, 2019. [Online]. Available: <https://doi.org/10.1016/j.pecs.2019.01.001>
- [53] S. B. Vilsen and D. I. Stroe, "Transfer Learning for Adapting Battery State-of-Health Estimation from Laboratory to Field Operation," *IEEE Access*, vol. 10, pp. 26 514–26 528, 2022.
- [54] F. Wang, Z. Zhai, Z. Zhao, Y. Di, and X. Chen, "Physics-informed neural network for lithium-ion battery degradation stable modeling and prognosis," *Nature Communications*, vol. 15, no. 1, pp. 1–12, 2024.

References

- [55] X. Yang, H. Xie, L. Zhang, K. Yang, Y. Liu, G. Chen, B. Ma, X. Liu, and S. Chen, "Early-stage degradation trajectory prediction for lithium-ion batteries: A generalized method across diverse operational conditions," *Journal of Power Sources*, vol. 612, no. May, p. 234808, 2024. [Online]. Available: <https://doi.org/10.1016/j.jpowsour.2024.234808>

Part II

Papers

